energies

MDPI

Article

Optimized Operating Strategy for the Thermal Management of a Battery Electric City Bus Using Bayesian Optimization

Henrik Schäfer *, Tobias Hellberg and Martin Meywerk

Automotive and Powertrain Engineering, Helmut Schmidt University, 22043 Hamburg, Germany; tobias.hellberg@hsu-hh.de (T.H.); martin.meywerk@hsu-hh.de (M.M.)

* Correspondence: henrik.schaefer@hsu-hh.de

Abstract

Electrified propulsion systems offer the potential to reduce global CO_2 emissions in the transportation sector, particularly in the field of urban mobility. Electric city buses combine the benefits of public transport systems with locally emission-free mobility. To ensure sufficient range for daily duty cycles, energy efficiency is crucial. Thermal management has a significant impact on the energy demand of battery electric vehicles. Therefore, efficiency can be improved by employing an integrated thermal management architecture that interconnects the individual coolant circuits and enables system-wide optimization. This study proposes an approach to optimize the operating strategy for the thermal management of a battery electric city bus. The important thermal components, including the drive system, battery system and HVAC system, are investigated. Experiments were carried out using a test setup of the system to identify the thermal behavior of the components. The study develops a simulation model of the thermal system of a BEV bus and subsequently uses this model to optimize the operating strategy by means of Bayesian optimization. The goal is to minimize energy demand under representative driving and environmental conditions in the city of Hamburg. The simulation-based analyses highlight potential gains resulting from the optimization of coolant temperatures and the flow rates of the components. Finally, a route- and temperature-based operating strategy is recommended.

Keywords: battery electric vehicle; electric city bus; thermal management; operating strategy; reduced energy demand; Bayesian optimization

1. Introduction

The reduction of greenhouse gas (GHG) emissions is a desirable goal. Electrification of the transportation sector is an option to reach locally emission-free mobility [1], and in the best case the reduction of GHG emissions, if alternative sources for electricity are used. The development of locally emission-free mobility focusses on several key areas. In addition to the development of energy-efficient vehicles, another key focus is on an efficient, low-emission strategy for powering these vehicles. New and innovative approaches highlight opportunities for optimizing the energy supply, for example, through solar energy [2]. Nevertheless, this article focuses on the consumer side and new developments in the area of vehicle energy efficiency. Especially in urban environments, the public transportation sector accounts for a large share of total traffic. In Europe, latest statistics show that newly registered electric buses account for a market share of over

Academic Editor: Marco Di Bartolomeo

Received: 23 September 2026
Revised: 28 October 2026
Accepted: 3 November 2026
Published: 4 November 2026

Copyright: © 2026 by the authors. Licensee MDPI, Basel, Switzerland. This article is an open access article distributed under the terms and conditions of the Creative Commons Attribution (CC BY) license.

25% [3]. This trend is primarily caused by battery electric city buses (BEV buses). Due to their high predictability regarding driving profiles and idle times, city buses offer ideal conditions for electric mobility with respect to thermal management and efficiency optimization. A key goal in the development of BEVs—whether passenger cars or commercial vehicles—is to increase energy efficiency. Higher efficiency either results in a longer driving range between charges, or it can reduce the battery capacity and, consequently, the cost and the weight of the vehicle [4]. In addition to the improvement of the component's efficiency—an area where there is little remaining potential due to the high level of technological advancement—thermal management is a key factor in the efficiency of BEVs and especially BEV buses [5–7]. The thermal system of a battery electric city bus comprises the electric drive system, the battery system and the heating, ventilation and air conditioning system (HVAC system). The different components have different thermal requirements, which must be combined to develop a thermal management system that meets the respective goals.

Firstly, there are different permissible temperature ranges for different components. When considering lithium-ion batteries (LIBs) as an energy storage system, a permissible temperature range could be roughly between 15 °C and 35 °C [8,9], but in detail the preferrable temperature range depends on many factors, e.g., chemistry or spatial temperature distribution. If these limits are exceeded, the performance of the battery is reduced, energy losses increase or safe operation cannot be guaranteed, as numerous studies have shown [10–14]. Moreover, warm temperatures especially have an influence on battery aging. Due to technological improvements in EV batteries or the implementation of thermal management systems, this effect can be reduced [15]. The electric drive system, specifically the inverter and the electric motor, has to be cooled, e.g., by a liquid coolant. The maximum temperature varies depending on the design and manufacturer and is usually not higher than 70 °C. The HVAC system must be designed to maintain a temperature of approximately 21 °C in the passenger compartment as well as the driver's front box, although the temperature may vary depending on the ambient temperature [16].

Secondly, the different components generate different heat flow profiles depending on the underlying load profile. These heat flow profiles must be considered when designing thermal systems, as they represent additional cooling requirements. The heat generated by the battery $\dot{Q}_{Bat}$ can be calculated by the joule heat $\dot{Q}_{jou}$ and the reversible heat $\dot{Q}_{rev}$. They depend on the battery current I, the open circuit voltage U_{OCV}, the battery voltage U_t and the cell temperature T, as shown in Equation (1) [17].

$$\dot{Q}_{Bat} = \dot{Q}_{jou} + \dot{Q}_{rev} = I \cdot \left(U_{OCV} - U_t\right) - I \cdot T \cdot \frac{\partial U_{OCV}}{\partial T}. \quad (1)$$

The heat flows of the inverter $\dot{Q}_{inv}$, converter $\dot{Q}_{con}$ and the electric motor $\dot{Q}_{mot}$ can be calculated based on the thermal losses of the systems. For simplicity, all component losses are assumed to be converted into heat within the respective thermal control volumes. [18]. The relations (for traction and recuperation mode) are shown in the following equations and are calculated by its electric power demand and its efficiency η:

$$\dot{Q}_{mot} = \begin{cases} (1-\eta_{mot}) \cdot P_{el,mot}, & P_{mech} \geq 0 \ \ (tract.), \\ (1-\eta_{mot}) \cdot P_{mech} & P_{mech} \leq 0 \ \ (recup.) \end{cases}, \tag{2}$$

$$\dot{Q}_{inv} = \begin{cases} (1-\eta_{inv}) \cdot P_{el,inv,in} & P_{mech} \geq 0 \ \ (tract.), \\ \left(\frac{1}{\eta_{inv}} - 1\right) \cdot P_{el,inv,out} & P_{mech} \leq 0 \ \ (recup.) \end{cases}, \tag{3}$$

$$\dot{Q}_{con} = (1-\eta_{con}) \cdot P_{el,con,in}. \tag{4}$$

The thermal requirements mentioned above illustrate the need for an adjustable, integrated thermal management system (TMS). Numerous studies reviewed different kinds of TMS, their characteristics and design differences [15,19–21]. Nevertheless, recent work mostly refers to either design optimizations of the thermal system [22,23] or thermal management strategies for passenger cars [24] or specific applications like delivery vehicles [25]. In addition to energy-related factors, an adjustable TMS can predict the battery's state, for example, in combination with data-driven approaches for estimating the state of health (SoH) [26].

This work describes a novel approach to model the thermal behavior of a reference system and includes an optimization of the operating strategy for the TMS of a battery electric city bus in order to reduce the overall energy demand. The system is based on design-improved thermal management, described in Schäfer et al. [27], in which the thermal liquid circuits of the components were combined to exploit synergy effects and increase efficiency. This paper proposes an improved simulation model for the described system, whose thermal behavior has been validated through experimental studies. The experimental procedures and their evaluation are described and quantified based on the calculation of characteristic values. The presented results demonstrate that the system can be modeled with a high degree of accuracy. Based on this model, a Bayesian optimization algorithm is used to identify an optimized operating strategy depending on boundary and load conditions like the driving profile and the ambient conditions. The environment described in this study refers to the city of Hamburg but can be applied to other use cases by adjusting these boundary and load conditions.

2. Modeling the Thermal System of a BEV Bus

The system under investigation involves the thermal components of a BEV bus, which are the drive system (motor and inverter), the battery system and the HVAC system. For simulative investigations, the components and their interactions are modeled in MATLAB/Simulink and MATLAB/Simscape (Version R2026a) (MathWorks, Natick, MA, USA) combined with an additional simulation of the HVAC system in Dymola (Dassault Systèmes, Vélizy-Villacoublay, FR) under usage of the TIL toolbox. An experimental setup in the laboratory of Automotive Engineering of Helmut-Schmidt-University (cf. [28]) is used for the calibration of the geometrical, physical and thermal parameters of the simulation model.

2.1. System Description

The reference system consists of specific standard components of a battery electric city bus. The drive system under investigation is the Voith Electrical Drive System (VEDS) (Driventic GmbH, Heidenheim a. d. Brenz, DE), which comprises the inverter,

the electric motor, the converter for supply of the low-voltage auxiliaries and the necessary control units as well as the power distribution and charging infrastructure. The motor, inverter and converter are liquid-cooled. The battery system considered here is the Webasto Commercial Vehicle (CV) Standard Battery System (Webasto SE, Stockdorf, DE) composed of six separate liquid-cooled battery packs and a Vehicle Interface Box (VIB) in the role of the battery management system (BMS). The HVAC system is an Eberspächer CO_2 heat pump AC138-125 HP (Eberspächer Sütrak GmbH & Co. KG, Renningen, DE). Eberspächer has also designed the TMS, which uses the heat energy supply from the HVAC system to bring the components to their optimal temperature range. Table 1 lists the key parameters of the system under investigation.

Table 1. Parameters for the system under investigation.

Drive System		Battery System		HVAC System	
Parameter	**Value**	**Parameter**	**Value**	**Parameter**	**Value**
max. power	P_{max} = 410 kW	capacity	C_{Bat} = 210 kWh	heating power	P_{heat} = 24 kW
dur. power	P_{dur} = 310 kW	nom. voltage	U_{nom} = 700 V	cooling power	P_{cool} = 34.3 kW
motor speed	n = 3800 rpm	max. power	P_{max} = 460 kW	refrigerant	CO_2
motor torque	M = 3100 Nm	Lithium-ion cells, prismatic NMC			
Central drive, no transmission					

The coolant supply of the individual components is realized by the thermal liquid circuits. Their volume flow rates are maintained by adjustable water pumps. The pump speeds and therefore the volume flow rates can be changed via Controller Area Network (CAN)-Bus. The HVAC system, besides its functionality to provide a comfortable temperature level to the passenger compartment and the driver's front box, delivers conditioned coolant (hot and cold) to the coolant tanks of the TMS. Switch valves are implemented to change between hot and cold coolant supply for each component. The connection between the TMS and the individual component's coolant circuits uses valves actuated by temperature-based control.

A control strategy is applied that opens each valve to reach the setpoint temperature for the component's coolant inlet. This temperature is set in the electronic control unit. In addition, a radiator is added within the coolant circuit of the drive system to meet the cooling requirements as much as possible. The schematic overview of the thermal liquid circuits and the TMS, described in a previous work [27] in detail, can be seen in Figure 1.

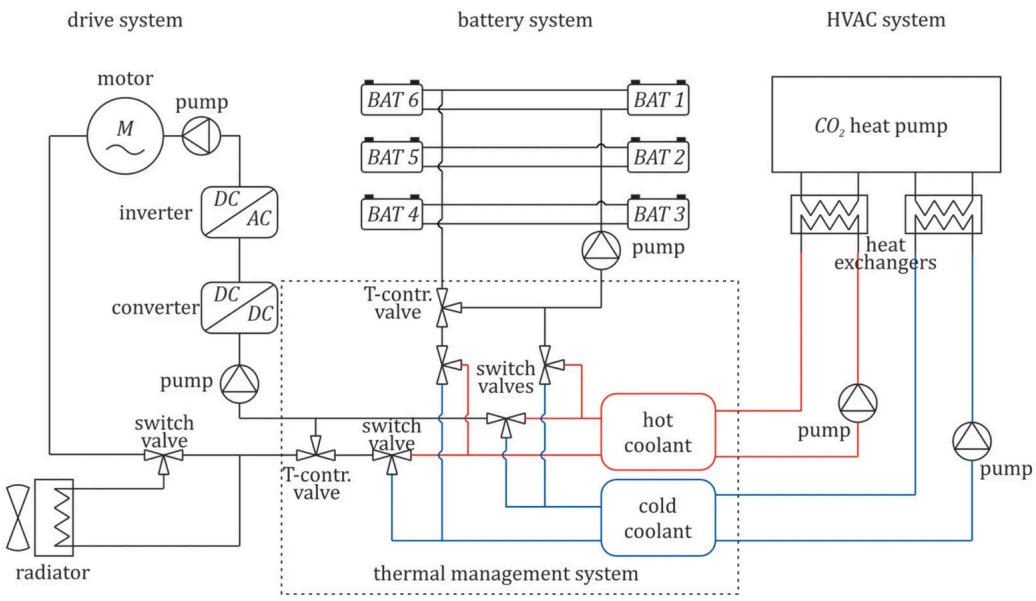


Figure 1. Schematic overview of the thermal liquid circuits and the thermal management system.

2.2. Simulation Model and Experimental Test Setup

The underlying modeling principle is a backward simulation using input signals based on a defined driving cycle in combination with vehicle parameters of an exemplary battery electric city bus. The simulation model is divided in three different subsystems: the mechanical subsystem, the electrical subsystem and the thermal subsystem. The mechanical subsystem calculates the mechanical power demand of the drive system from the specific driving cycle regarding the fundamental laws of longitudinal dynamics as described, e.g., in [29]. The necessary vehicle parameters of the representative BEV bus, precisely a 15 m solo bus, are shown in Table 2.

Table 2. Assumption of vehicle parameters for an exemplary BEV bus (15 m solo bus).

Parameter	Value (15 m Solo Bus)
vehicle weight	m_{veh} = 15.000 kg [1]
rolling resistance coefficient	f_r = 0.005 [30]
aerodynamic drag force coefficient	c_d = 0.4 [31]
cross sectional area	A = 7 m^2 [31]
rotational mass factor	λ_i = λ = 1.05 [32]

[1] Mean value calculated from actual measurement data.

The electric power demand of the drive system $P_{el,VEDS}$ is calculated from the mechanical power demand and the characteristic maps of motor and inverter. As described above, the losses of the components are assumed to be thermal losses. The power demand of the auxiliaries $P_{el,aux}$ is assumed to be constant. The demands $P_{el,VEDS}$ and

$P_{el,aux}$ are added to the demand of the HVAC system $P_{el,HVAC}$, which is calculated by the relation between ambient temperature and required thermal demand $\dot{Q}_{therm,HVAC}$ of the HVAC system and the Coefficient of Performance (COP) of the HVAC system to calculate the overall power demand $P_{el,Bat}$:

$$P_{el,Bat} = P_{el,VEDS} + P_{el,aux} + \dot{Q}_{therm,HVAC} \cdot \frac{1}{COP_{HVAC}}. \quad (5)$$

These parameters are input signals for the electrical and the thermal subsystem. The electrical subsystem calculates the characteristic electric values battery current I, battery voltage U_{Bat} and State of Charge SoC. For this purpose, characteristic maps of the battery system are used, which describe the cell voltage as well as the internal resistance depending on SoC and cell temperature. The thermal subsystem models the thermal behavior of the components, in particular, their heat generation and the resulting temperatures. The heat generations are calculated with the relations described in Equations (1)–(4). The cell temperature increase of the battery system is modeled by the thermal mass M_{th} and the voltage drop $V_{T,i}$ as well as the internal resistance $R_{T,i}$ for each cell:

$$M_{th} \cdot \frac{dT}{dt} = \sum_i \frac{V_{T,i}^2}{R_{T,i}}. \quad (6)$$

The temperature increase of the drive system components is simplified by their heat flow $\dot{Q}_{comp}$, the component's mass m_{comp} and their specific heat capacity c_{comp}:

$$\frac{dT}{dt} = \frac{\dot{Q}_{comp}}{m_{comp} \cdot c_{comp}}. \quad (7)$$

Different parameters are needed for the calculations in the simulation model. For this reason, different sources of parametrization are implemented, which can be seen in the overview in Figure 2. First, the characteristic maps and technical key figures are taken by the manufacturer's datasheets. In addition, the thermal behavior of the HVAC system as well as the heating and cooling curves of the coolant tanks of the TMS are modeled in Dymola and implemented via a functional mock-up interface (fmi). The passenger compartment and the driver's front box are not modeled in detail. Instead, their thermal energy demand is accounted for using the empirically determined characteristic curves described above, depending on the ambient temperature. A more detailed description of the simulation model and the underlying calculations can be found in Schäfer et al. [28].

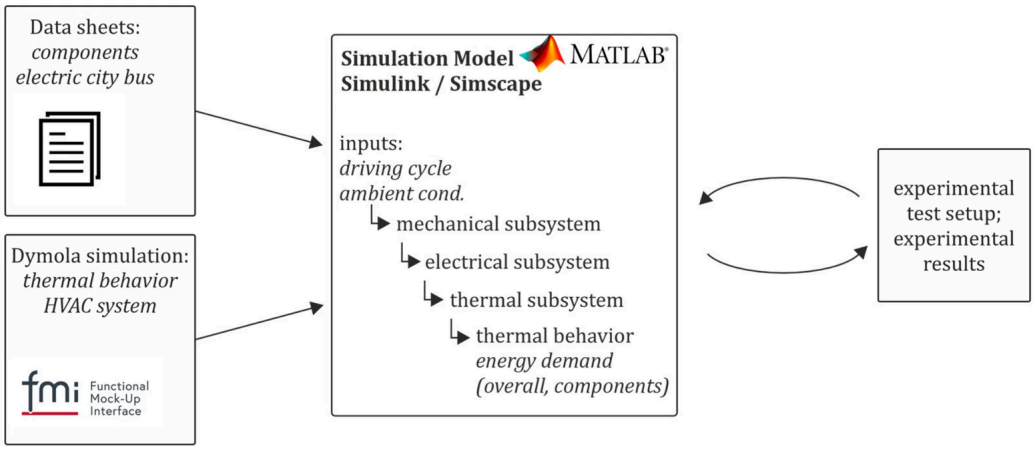


Figure 2. Structure and parameter sources of the simulation model including interaction with experimental results (iterative approach).

The simulative investigation is validated by experimental results. The experimental investigation for validation processes is realized in a test setup on the institutes' power and inertia simulator (PAISI). The test setup comprises all described components as well as the thermal circuits of the different systems. The test setup offers the ability to subject the system to defined driving cycles. A longitudinal dynamics calculation combined with calculation of inertia computes the driving resistances. The test setup with the individual components labeled can be seen in Figure 3.

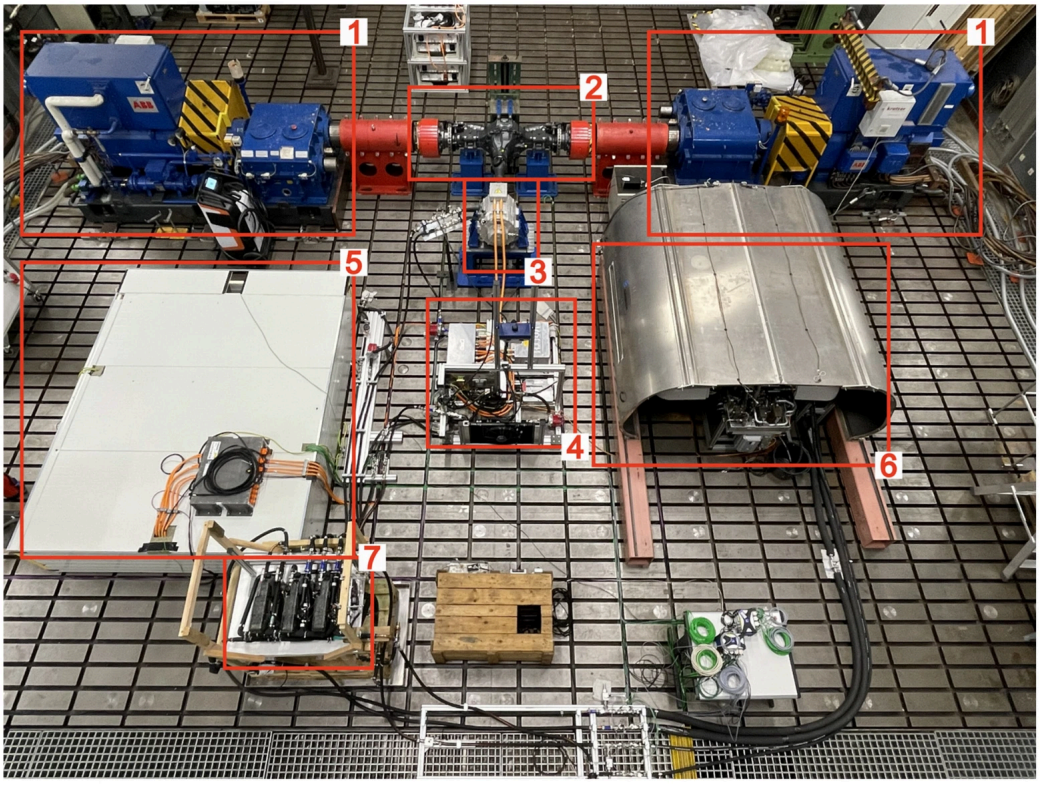


Figure 3. Test setup for experimental validation of the system with components labeled: (1) ABB machines (PAISI); (2) axle; (3) electric motor; (4) power electronics; (5) battery system; (6) HVAC system; (7) thermal management system.

2.3. Validation of the Simulation Model

The modeling results have already been partially validated experimentally in earlier studies [27,33]. In these studies, the validation focused on a split thermal management system with separate thermal solutions for the battery system and the powertrain. Experiments were conducted to validate the thermal behavior of the components. Due to its high thermal inertia, the battery system was preconditioned, and the experiments were conducted at both cold and warm initial temperatures. A comparison between simulation values and experimental results shows a high degree of accuracy [28,33]. However, the system under investigation in this research is based on an improved thermal management system. Therefore, this study aims to validate the results of the improved system.

The experiments are conducted using six different driving cycles, which are described in the following chapter, and moderate ambient temperatures ($T_{amb} \approx 20\ ^\circ\mathrm{C}$). The results of the most important variables of the three different subsystems are shown in Figure 4. Various performance metrics describing the deviation between simulative and experimental results are calculated to evaluate the accuracy of the simulation model. These include R^2, $RMSE$ and MAE.

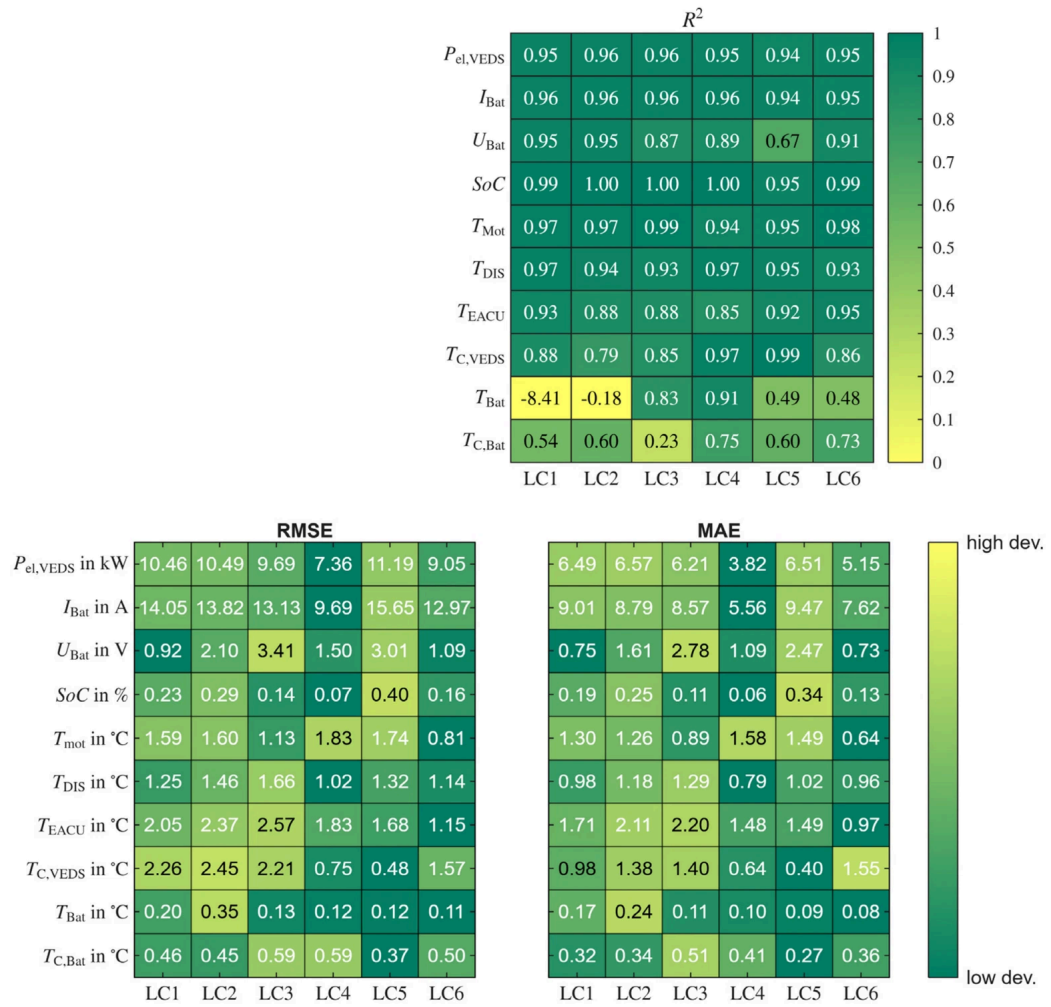


Figure 4. Evaluation of the experimental validation. simulative results of the three subsystems regarding the operating principle of the TMS in warm ambient conditions.

The various metrics were selected based on the different behavior of the data points

in order to achieve a comprehensive overall assessment. The R^2 values indicate a high degree of accuracy for the mechanical and electrical subsystems as well as for the thermal subsystem of the drive system. However, due to the battery system's high thermal inertia, R^2 yields poor results for its thermal behavior. The analysis shows low thermal gradients for the battery system during a driving cycle. The inclusion of *RMSE* and *MAE* indicates that the absolute error for the battery system is very low.

2.4. Simulative Investigation

The following evaluation in Figure 5 shows exemplary simulative results for important key figures of the described subsystems and especially the operating principle of the TMS. The input parameters in this test are a specific driving cycle and warm ambient conditions.

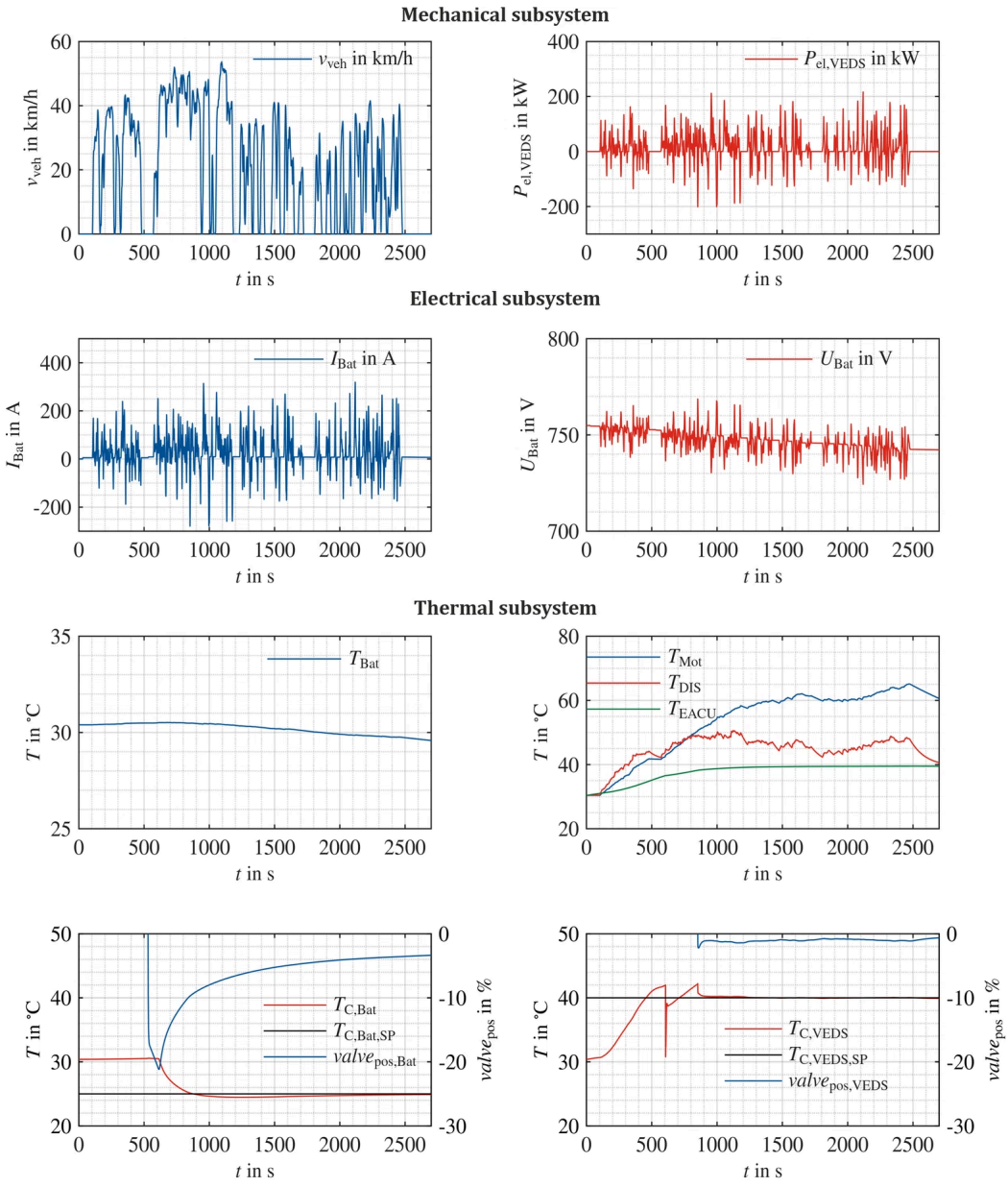


Figure 5. Exemplary simulative results of the three subsystems regarding the operating principle of the TMS in warm ambient conditions.

An overview of the mechanical subsystem shows the velocity profile $v_{veh}(t)$ and the calculated power demand $P_{el,VEDS}(t)$ resulting from the longitudinal dynamics model. The battery current $I_{Bat}(t)$ arises out of this power demand, the additional power demand of further components like auxiliaries $P_{el,aux}$ and the HVAC system $P_{el,HVAC}$ and the modeled battery voltage U_{Bat}:

$$I_{Bat} = \frac{P_{el,VEDS} + P_{el,aux} + P_{el,HVAC} + P_{el,HVAC,add}}{U_{Bat}}. \quad (8)$$

In this case, $P_{el,HVAC}$ describes the energy demand of the HVAC system to fulfill the thermal demand of the cabin. In addition, $P_{el,HVAC,add}$ includes the additional power demand for the TMS calculated from the mass flow $\dot{m}_{TMS}$, the specific heat capacity of the coolant $c_{p,coolant}$ and the temperature difference ΔT_{TMS} of the TMS:

$$P_{el,HVAC,add} = \dot{m}_{TMS} \cdot c_{p,coolant} \cdot \Delta T_{TMS} \cdot \frac{1}{COP_{HVAC}}. \quad (9)$$

Further evaluations show the temperatures of the components as well as the operating profile of the TMS by the temperature control valve positions for both liquid cooling cycles. The variable valve position is controlled by the value: $0\%\ (closed) > valve_{pos} > -100\%\ (opened)$. Moreover, the setpoint temperatures (SPs) and the coolant inlet temperatures are shown.

The results describe the ability of the TMS to control the coolant inlet temperatures of the components according to their SP in high accuracy. Moreover, the analysis of the thermal behavior shows that the control of the coolant temperatures has an influence on the component temperatures. The battery temperature T_{Bat} is reduced (due to its high thermal inertia with a small gradient) and the temperatures of the drive system components T_{mot}, T_{DIS} and T_{EACU} are kept nearly constant after activation of the TMS. Moreover, an important fact regarding the operating strategy of the TMS can be seen: Within the control strategy, it is not foreseen to heat the coolant circuit of the drive system externally due to self-heating of the components. The activation of the TMS only represents the cooling demand of the drive system when exceeding the setpoint temperature.

3. Optimization

3.1. Boundary Conditions

The goal of this study is to develop an optimized operating strategy for the TMS of the electric city bus depending on the boundary conditions, which are driving profile and ambient conditions. Therefore, these conditions must be defined for this study. In previous work, representative driving cycles for BEV buses have been defined using measurement data of the city of Hamburg [27]. The database contains more than 4000 individual driving cycles that are processed by a methodical approach including the definition of characteristic values, dimension reduction and a cluster analysis to identify six representative driving cycles (Load Case 1–Load Case 6). The cycles, including the vehicles' velocity profile $v_{veh}(t)$ and the altitude profile, can be seen in Figure 6.

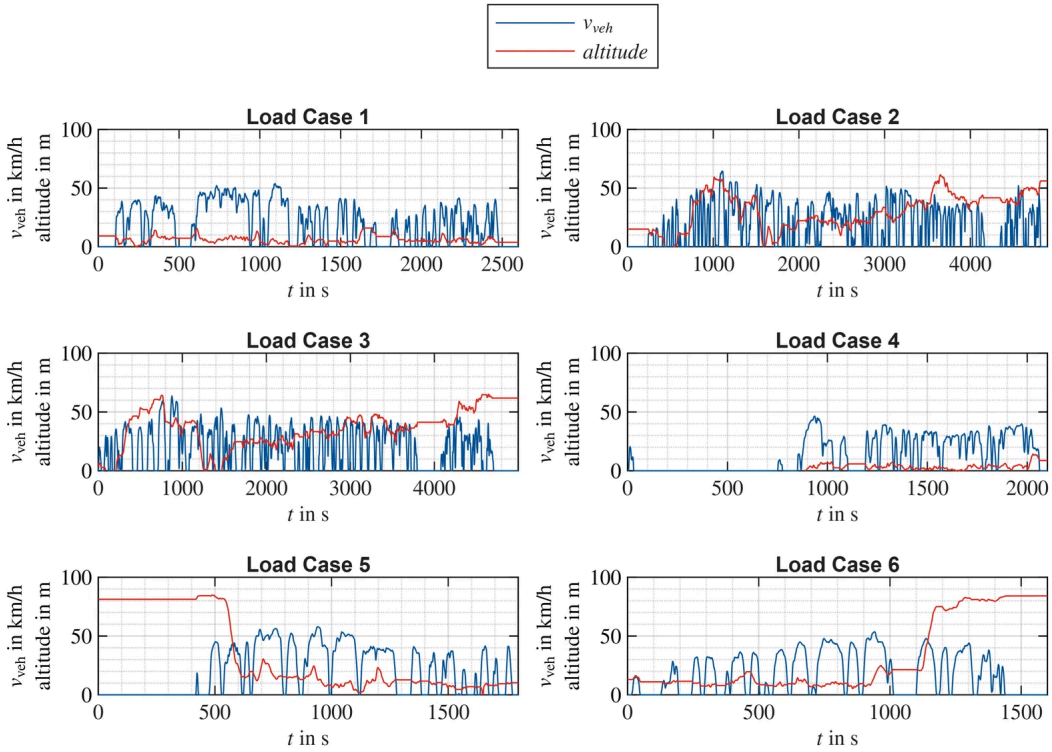


Figure 6. Driving cycles (Load Case 1–Load Case 6) for further investigations. Cycles are defined by a methodical analysis of real driving profiles in the city of Hamburg ($n_{Cycle} \approx 4000$).

The characterization of the different representative load cases has been done in previous work by Schäfer et al. and is listed below [27]:

- Load Case 1: medium duration, low-demanding topography, high average speed;
- Load Case 2: high duration and trip distance, demanding topography, high dynamics, high number of stops;
- Load Case 3: high duration and trip distance, demanding topography, high dynamics, high idle times;
- Load Case 4: medium duration, low-demanding topography, low dynamics, low average speed, high idle times;
- Load Case 5: low duration and trip distance, demanding topography, high idle times;
- Load Case 6: low duration and trip distance, demanding topography, short idle

times.

To determinate the ambient conditions, an analysis of climate data for the city of Hamburg was conducted. The ambient temperatures recorded by the Deutscher Wetterdienst (DWD) at measuring station No. 1975 (Hamburg-Fuhlsbüttel) over a 50-year period (1976–2025) are analyzed and examined [34]. To eliminate extreme individual events, the 1%- and 99%-percentile of the temperatures are considered. Figure 7 shows the evaluation of the climatic data including the 1%- and 99%-percentiles and the 25%- and 75%-boxplots of the temperature distribution for each month.

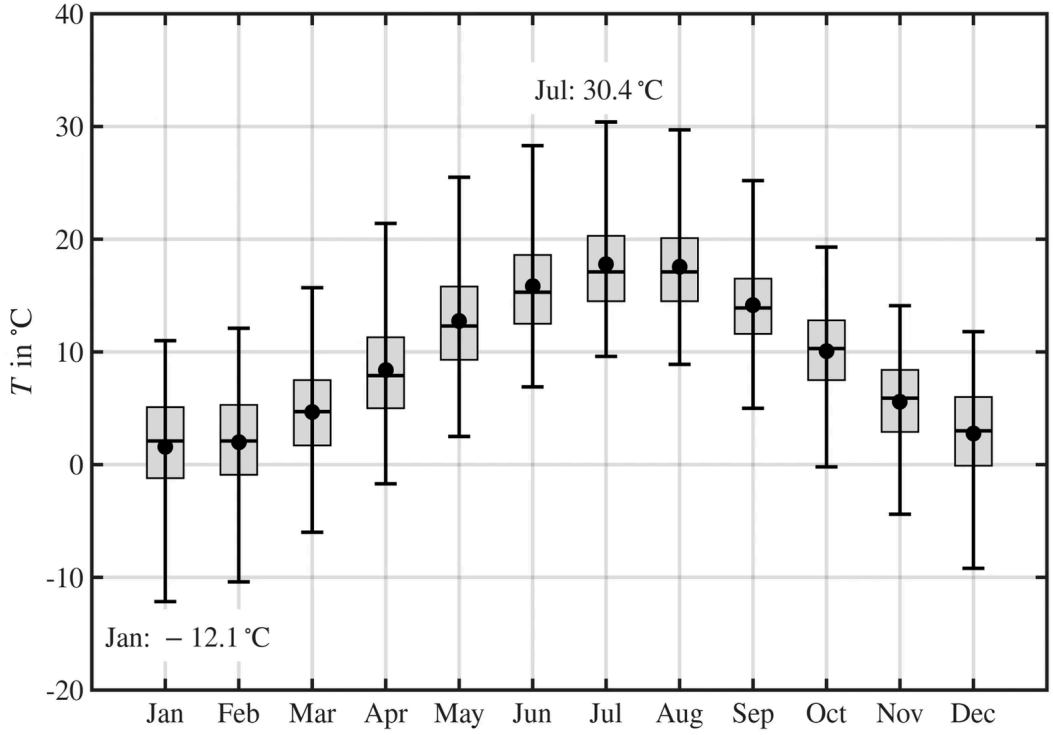


Figure 7. Analysis of climatic data for the city of Hamburg over the past 50 years (1976–2025). Measurement station based in Hamburg-Fuhlsbüttel (No. 1975) [34].

From the six load cases and the minimum and maximum temperature, twelve test cases can be defined. The test matrix for optimization is defined in Table 3.

Table 3. Test matrix with details for definition and nomenclature of test cases.

Basic Driving Cycle	$T_{amb} = -12.1$ °C	$T_{amb} = 30.4$ °C
Load Case 1	Opt _1_cold	Opt_1_warm
Load Case 2	Opt_2_cold	Opt_2_warm
Load Case 3	Opt_3_cold	Opt_3_warm
Load Case 4	Opt_4_cold	Opt_4_warm
Load Case 5	Opt_5_cold	Opt_5_warm
Load Case 6	Opt_6_cold	Opt_6_warm

3.2. Optimization Algorithm

The optimization problem is defined by an expensive solution of the objective function since the objective function consists of the time-consuming simulation model in MATLAB/Simulink and Simscape. Moreover, it shows nonlinear behavior because of the

dynamic simulation including differential equations, switching processes (e.g., valves) and other nonlinear thermal relations as described in [35]. Many well-known optimization methods do not fit non-linear objective functions and high amounts of constraints [36]. One common method to solve the described optimization problems is the Bayesian optimization algorithm. Bayesian optimization is advantageous for non-linear, time-consuming objective function, as mentioned in numerous studies [37–41].

The Bayesian optimization algorithm uses a probabilistic surrogate model, mostly a Gaussian Process (GP) model, which approximates the objective functions and the constraints. It combines a mean function and a covariance function and assumes a multivariate Gaussian distribution of the observed data [42]. The solution of the Bayesian Optimization including the GP model can be done in MATLAB.

The decision where to search for the optimum of the objective function is defined by the Acquisition Function (AF) that refers to the balance between two different methods, exploration and exploitation. Exploration searches among values with high uncertainty whereas exploitation tries to investigate areas with high optimality. There are different forms of AFs that can be found in the literature [40,42]. In this case, the Expected Improvement (EI) method should be used, which calculates the expected improvement with respect to the optimum obtained so far depending on the input signals and the objective function [40].

3.3. Optimization Problem

The optimization problem in this work is a typical minimization problem. The overall energy demand $E_{el,Bat}$ should be minimized according to six different constraints or optimization variables. The overall energy demand of the system is defined by the energy demand used for tractive effort of the vehicle $E_{el,tract}$, the energy demand of the auxiliaries $E_{el,aux}$, the energy demand of the HVAC system $E_{el,HVAC,cabin}$ for conditioning the cabin and the energy demand of the thermal system $E_{el,therm.}$. The calculation of the energy demands is described in Equations (10)–(14).

$$E_{el,Bat} = \int_0^{t_{abs}} \begin{cases} \frac{1}{\eta_{Bat}} \left(P_{el,tract} + P_{el,aux} + P_{el,HVAC,cabin} + P_{el,therm.} \right), & E_{el,Bat} \geq 0 \ \ (discharging), \\ \eta_{Bat} \left(P_{el,tract} + P_{el,aux} + P_{el,HVAC,cabin} + P_{el,therm.} \right), & E_{el,Bat} \leq 0 \ \ (charging) \end{cases} dt, \tag{10}$$

$$E_{el,tract} = \int_0^{t_{abs}} P_{el,VEDS}(t) \ dt, \tag{11}$$

$$E_{el,aux} = \int_0^{t_{abs}} P_{el,aux}(t) \ dt, \tag{12}$$

$$E_{el,HVAC,cabin} = \int_0^{t_{abs}} \dot{Q}_{therm,HVAC}(t) \cdot \frac{1}{COP_{HVAC}} dt, \tag{13}$$

$$E_{el,therm.} = \int_0^{t_{abs}} \dot{Q}_{TMS}(t) \cdot \frac{1}{COP_{HVAC}} dt = \int_0^{t_{abs}} \dot{m}_{TMS}(t) \cdot c_{p,coolant} \cdot \Delta T_{TMS} \cdot \frac{1}{COP_{HVAC}} dt \ . \quad (14)$$

The energy demand used for traction depends on the driving cycle (Load Case) and the ambient conditions, especially the ambient temperature T_{amb}. Moreover, the drive system's efficiency is linked to the component temperature. The component temperature can be controlled by its coolant circuit and therefore depends on the coolant inlet temperature $T_{C,VEDS,in,SP}$. The energy demands of the auxiliaries and the HVAC system are defined by the ambient conditions but also by the length of the driving cycle t_{abs} and therefore the duration of activation of the low-voltage system and the HVAC system. The interdependencies can be seen in Equations (15)–(17).

$$E_{el,tract} = f\left(v_{veh}(t),\ gradient(t), T_{amb}, T_{C,VEDS,in,SP}\right), \quad (15)$$

$$E_{el,aux} = f\left(t_{abs}, T_{amb}\right), \quad (16)$$

$$E_{el,HVAC,cabin} = f\left(t_{abs}, T_{amb}\right). \quad (17)$$

The energy demands of the auxiliaries and the HVAC system are assumed to be constant, depending on their dependencies within an analyzed optimization run. Thus, the energy demand of the thermal system should be minimized. The design variables are the setpoints for the coolant inlet temperatures of drive system $T_{C,VEDS,in,SP}$ and battery system $T_{C,Bat,in,SP}$, the pump factors of both systems, which correlate with the volume flow rates $f_{pump,C,VEDS,in}$, $f_{pump,C,Bat,in}$ and the volumes of the TMS tanks for cold water $V_{C,CW,tank}$ and hot water $V_{C,HW,tank}$. These variables are combined in the vector $\boldsymbol{x}$, as mentioned in Equation (18). The design variables are constrained by the lower and upper bounds. These bounds depend on technical thresholds or physical limits as well as constructive restrictions and are shown in Table 4. The limits on coolant temperatures are directly related to the component's temperature limits. For various reasons, these temperatures are controlled by the coolant inlet temperatures. First, the model's control strategy applies to the actual system on the test bench. This system allows the inlet temperatures to be set via a setpoint signal. Furthermore, previous investigations have confirmed that the technical limits of the component temperatures can be monitored by adjusting the coolant temperatures. Due to its high thermal inertia, the temperature of the battery system follows the coolant temperature with a delay. Due to the increased cooling requirements of the components, the temperature of the drive system is more dynamic and measurably higher than the coolant temperature. Taking this effect into account, the selected limit values for the drive system are low to ensure that

the maximum temperatures are not exceeded.

Table 4. Lower and upper bounds for the optimization variables according to technical thresholds and physical limits.

Lower Bound	Optimization Variable	Upper Bound
30 °C	$T_{C,VEDS,in,SP}$	50 °C
15 °C	$T_{C,Bat,in,SP}$	35 °C
0.8	$f_{pump,C,VEDS,in}$	1.2
0.8	$f_{pump,C,Bat,in}$	1.2
1 l	$V_{C,CW,tank}$	10 l
1 l	$V_{C,HW,tank}$	10 l

The optimization problem is defined in Equation (19) by its objective function f, the design variables and their constraints.

$$\boldsymbol{x} = \begin{bmatrix} T_{C,VEDS,in,SP} \\ T_{C,Bat,in,SP} \\ f_{pump,C,VEDS,in} \\ f_{pump,C,Bat,in} \\ V_{C,CW,tank} \\ V_{C,HW,tank} \end{bmatrix} \tag{18}$$

$$\begin{aligned} &\min_{\boldsymbol{x}} \; E_{el,Bat}(\boldsymbol{x}) \\ &\text{subject to } \boldsymbol{x}^{lower} \leq \boldsymbol{x} \leq \boldsymbol{x}^{upper}. \end{aligned} \tag{19}$$

The optimization is performed using the Bayesian optimization algorithm in MATLAB. The algorithm is defined by its parameters, such as a maximum iteration number of 200, an amount of 20 initial and random calculations and the definition of the acquisition function. In this case, the expected improvement plus method is used, a MATLAB defined variation of the expected improvement method. The optimization procedure including all test cases is shown in Figure 8.

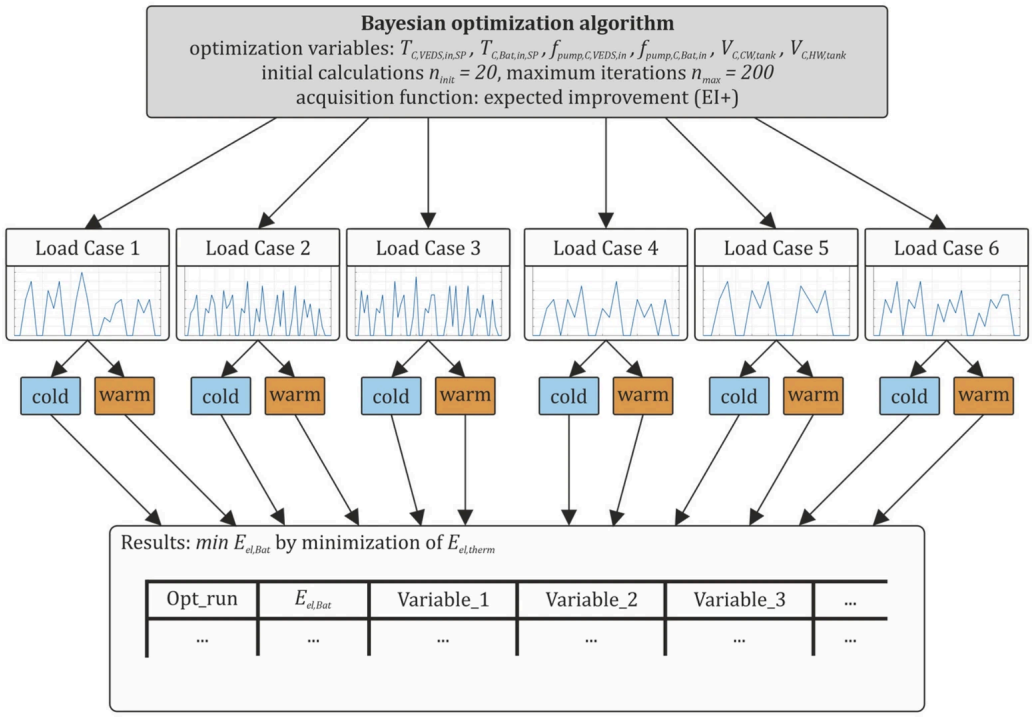


Figure 8. Optimization procedure and conditions of the Bayesian optimization algorithm.

4. Results

The optimization procedure describes twelve optimization results. The first part of the evaluation focuses on the optimization algorithm and the quality of the results. The second part compares the optimization results of all runs to define optimal values for the optimization variables.

4.1. Evaluation of Optimization Quality and Significance of the Results

Figure 9 shows the results of the optimization for Opt_1_cold and Figure 10 shows the results for Opt_1_warm. Further optimization results can be found in Appendix A. Results show the calculated energy demand depending on the different optimization runs (a) and the coverage of the variable space (b). Additionally, the percentage of valid simulations is mentioned as there is a possibility that single simulations gain errors due to specific selection of the optimization variables.

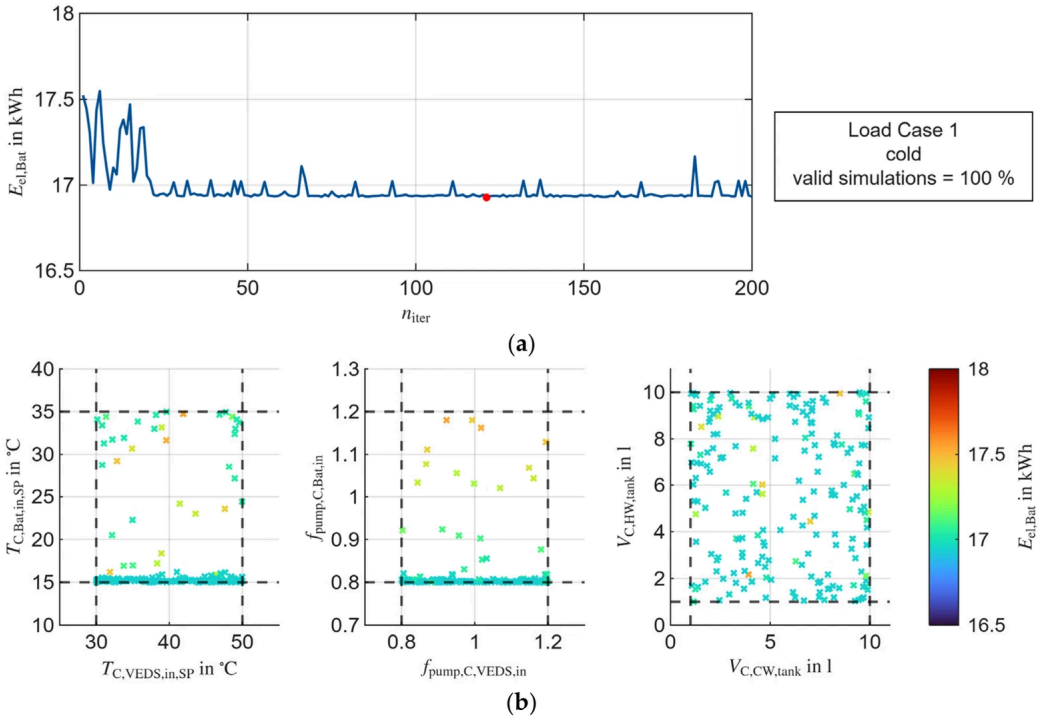


Figure 9. Results of the optimization for Load Case 1 at cold ambient conditions (Opt_1_cold): (**a**) calculated energy demand $E_{el,Bat}$ for all iterations; (**b**) energy demand $E_{el,Bat}$ depending on the different variable spaces.

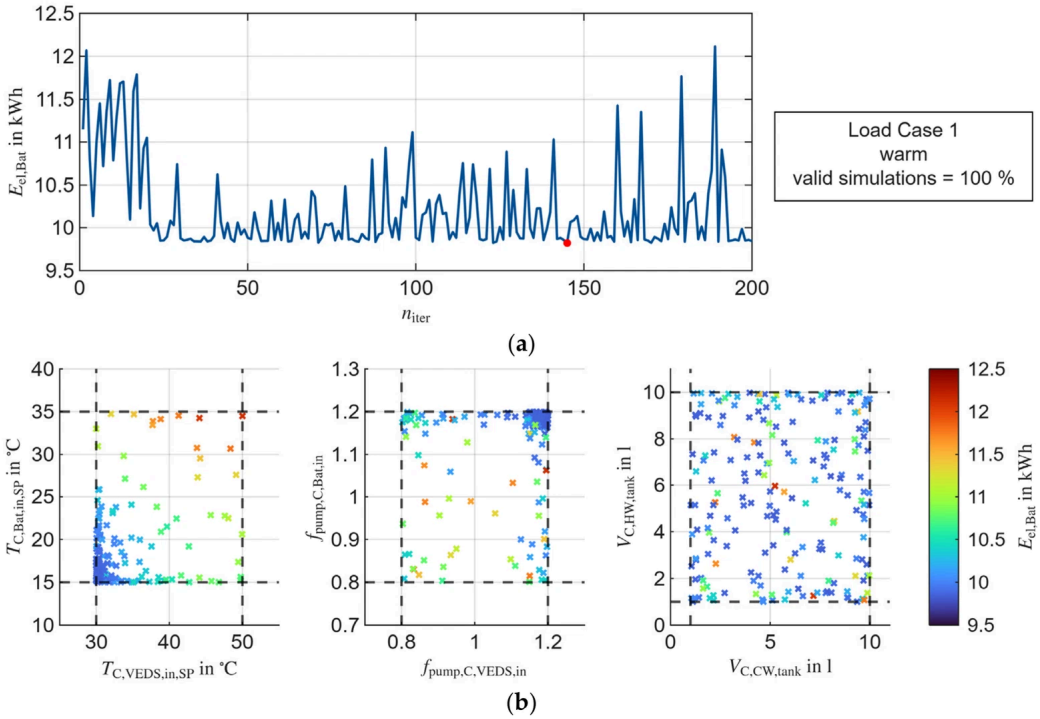


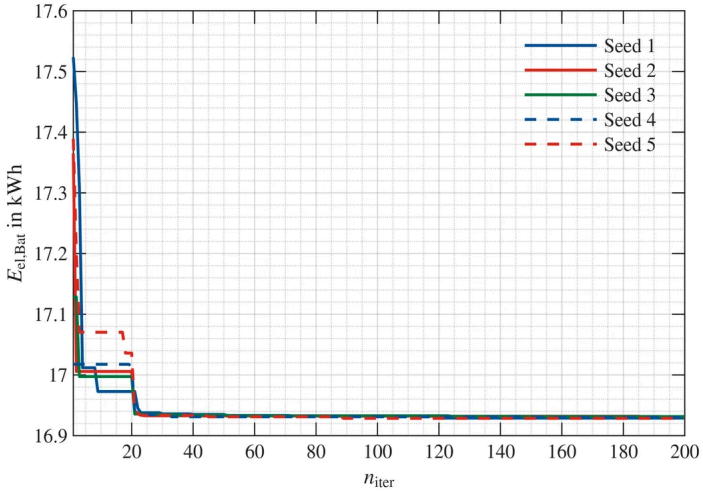
Figure 10. Results of the optimization for Load Case 1 at warm ambient conditions (Opt_1_warm): (**a**) calculated energy demand $E_{el,Bat}$ for all iterations; (**b**) energy demand $E_{el,Bat}$ depending on the different variable spaces.

For Opt_1_cold, it can be observed that the variation in the energy demand over the

iterations is minor compared to Opt_1_warm. The warm conditions cause higher deviations in energy demand, depending on the optimization variables. This behavior is analogous to the other optimizations under the influence of other load cases. Furthermore, the results show, especially in the Appendix, that the optimum can be found in different iterations. The improvement of the best-so-far values between iteration 100 and iteration 200 is < 0.1%. The diagrams in Figures 9b and 10b show the calculated energy demand depending on the optimization variables in the constrained variable space. The evaluation shows three important findings that correspond to the additional analyses in Appen dix A:

- An assertion on the quality of the investigation of the variable space can be formulated. The amount of 200 iterations fills the space under investigation for all variables. Therefore, the overall quality of the optimization can be considered sufficient. This leads to a positive conclusion regarding the scope of the investigation under the given parameters.
- For cold ambient conditions, a decrease in the energy demand can be reached by reducing the battery pump factor $f_{pump,C,Bat,in}$ and therefore the volume flow rate. Moreover, there is a correlation between high battery setpoint temperatures $T_{C,Bat,in,SP}$ and low energy demands at cold ambient conditions, which is not a hundred percent resilient. Other variables show a minor influence at cold conditions.
- For warm ambient conditions, the lowest energy demand can be identified in combination with high setpoint temperatures $T_{C,VEDS,in,SP}$ and $T_{C,Bat,in,SP}$. Moreover, a slight correlation between low energy demands and lower pump factors $f_{pump,C,VEDS,in}$ and $f_{pump,C,Bat,in}$ can be assumed.

To evaluate the convergence behavior and reproducibility of the Bayesian optimization, five exemplary optimization runs were conducted using different random seeds. Each run comprises 200 objective function evaluations. The results are shown in Figure 11. The evaluation demonstrates a rapid reduction in the objective function during a small amount of iterations. Only marginal improvements were observed during the remaining evaluations. It is shown that the objective function values are largely insensitive to the random initialization for the investigated conditions. The results suggest that 200 iterations provide a conservative approach for the investigated test. However, the observed behavior does not constitute mathematical proof of convergence to the global optimum.



Test	$\Delta E_{el,Bat\ 100\text{-}200}$
Opt_1_cold Seed 1	0.019 %
Opt_1_cold Seed 2	0.006 %
Opt_1_cold Seed 3	0.008 %
Opt_1_cold Seed 4	0.006 %
Opt_1_cold Seed 5	0.000 %

Figure 11. Convergence histories of exemplary optimization runs (Opt_1_cold) performed with five different seeds. Relative improvement of the objective function value between iterations 100 and 200.

Considering that a single iteration lasts between 120 and 300 s, depending on the driving cycle, the total duration for 200 iterations in the test setup used is 6.6 to 16.6 h. Therefore, the conservative approach is a sufficient compromise between improvement and computational costs.

In the next step, a correlation analysis was conducted to determine the influence of the parameters on the overall energy demand. The Spearman correlation is used to evaluate the optimization variables with highest and lowest correlation. The Spearman correlation calculates a unitless factor $S \in [-1, 1]$. Positive correlation is linked to a positive Spearman factor, and negative correlation is linked to a negative Spearman factor [43]. The results for all twelve test cases are shown in Figure 12.

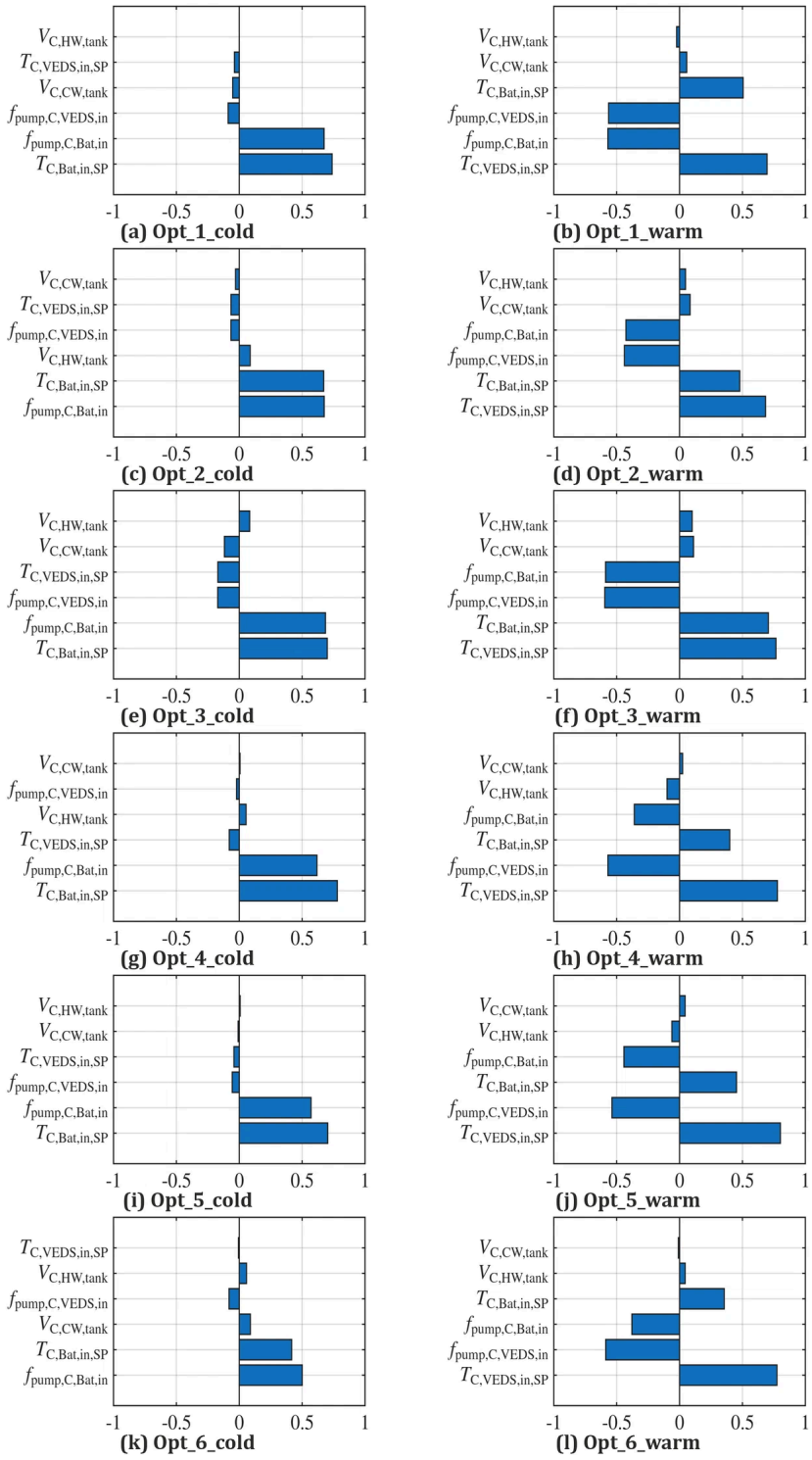


Figure 12. Results of the Spearman correlation analysis (correlation between the variables and the energy demand).

Four key findings can be determined by evaluation of the sensitivity analyses in Figure 10:

- The variables of the VEDS cooling circuit ($T_{C,VEDS,in,SP}$, $f_{pump,C,VEDS,in}$) show weaker correlations to the energy demand in cold ambient conditions compared to the variables of the battery cooling circuit ($T_{C,Bat,in,SP}$, $f_{pump,C,Bat,in}$);

- Both setpoint temperatures $T_{C,VEDS,in,SP}$ and $T_{C,Bat,in,SP}$ have stronger correlation to the energy demand at warm ambient conditions;
- The pump factors (and therefore the volume flow rates), especially for the battery circuit $f_{pump,C,Bat,in}$, have strong correlation at cold ambient conditions;
- Tank volumes $V_{C,CW,tank}$ and $V_{C,HW,tank}$ have weak correlation to the energy demand regardless of the ambient temperatures.

The comparatively low correlation coefficients for tank volumes suggest that, under the examined optimization conditions, these parameters are less strongly correlated with fluctuations in energy demand. However, this observation does not establish that their physical influence is negligible, as nonlinear relationships and interactions with other parameters may not be captured by the correlation analysis. Therefore, tank volumes are not considered in the correlation-based analysis of the dominant optimization variables. This limitation serves to focus the interpretation of the model under investigation and does not imply that the tank volumes in the TMS can generally be disregarded.

4.2. Optimization Results

If the tank volumes do not affect the energy demand in a significant way, the definition of optimum variable values should focus on the temperatures and the pump factors. These variables are software-defined parameters. The setpoint temperatures as well as the pump factors can be set in the control strategy via CAN-Bus. Therefore, an optimization of the system can be done easily, depending on spontaneous changes in the operating point of the BEV bus.

Table 5 shows the optimized values calculated by the Bayesian optimization.

Table 5. Optimization results: optimal values for optimization variables.

Test Case	$T_{C,VEDS,in,SP}$ in °C	$T_{C,Bat,in,SP}$ in °C	$f_{pump,C,VEDS,in}$	$f_{pump,C,Bat,in}$
Opt_1_cold	37.41	15.01	0.91	0.80
Opt_2_cold	35.95	15.05	1.10	0.80
Opt_3_cold	39.41	15.02	1.06	0.80
Opt_4_cold	46.23	15.14	0.91	0.80
Opt_5_cold	36.73	15.10	1.09	0.80
Opt_6_cold	44.34	15.03	1.14	0.80
Opt_1_warm	30.13	15.41	1.19	1.20
Opt_2_warm	30.14	15.36	1.19	1.20
Opt_3_warm	30.14	15.59	1.19	1.20
Opt_4_warm	30.11	16.08	1.18	1.20
Opt_5_warm	30.09	15.02	1.19	1.20
Opt_6_warm	30.32	15.87	1.20	1.20

5. Discussion

Each combination of optimized variables correlates with an optimized value for the

overall energy demand $E_{el,Bat}$. Table 6 shows the optimized energy demand in comparison to a baseline configuration. The baseline configuration of the operating strategy was described in [27] in the context of the introduction of the TMS design change. It consists of the average values between the upper and lower bounds of the constraints and is defined by the operating strategy used for validation tests. This baseline configuration is defined by the following:

Table 6. Optimization results: potential energy savings by an optimized operating strategy in comparison to the baseline scenario.

Test Case	Optimized $E_{el,Bat}$ in kWh	Baseline $E_{el,Bat}$ in kWh	$\Delta E_{el,Bat}$ in %
Opt_1_cold	16.9290	17.2790	2.03
Opt_2_cold	32.3378	33.0246	2.08
Opt_3_cold	32.2425	32.9271	2.08
Opt_4_cold	10.9773	11.1787	1.80
Opt_5_cold	8.8621	8.9789	1.30
Opt_6_cold	10.9970	11.0707	0.67
Opt_1_warm	9.8233	10.8723	9.65
Opt_2_warm	19.6603	21.2421	7.45
Opt_3_warm	19.7902	21.3551	7.33
Opt_4_warm	5.9865	6.8700	12.86
Opt_5_warm	4.5435	5.3971	15.82
Opt_6_warm	7.0018	7.8300	10.58

- Setpoint temperatures $T_{C,VEDS,in,SP} = 40\ ^\circ\mathrm{C}$; $T_{C,Bat,in,SP} = 25\ ^\circ\mathrm{C}$;
- Pump factors $f_{pump,C,VEDS,in} = f_{pump,C,Bat,in} = 1$.

The percentage improvement is calculated in Equation (20) and describes the overall energetic potential of the optimized operating strategy.

$$\Delta E_{el,Bat} = \frac{E_{el,Bat,baseline} - E_{el,Bat,optimized}}{E_{el,Bat,baseline}} \cdot 100\,\%. \quad (20)$$

The evaluation of the energetic improvement $\Delta E_{el,Bat}$ shows mean values of 1.66% for cold ambient conditions and 10.61% for warm ambient conditions. The difference can be explained by the operating strategy of the VEDS coolant circuit, which is not externally heated and therefore has no energy demand in cold conditions. Moreover, the variance in energy demand within one test case is higher for warm ambient conditions, as described in Figure 9a and Figure 10a and in Appendix A. For this reason, the potential for energy savings is higher at warm ambient conditions under the influence of different operating strategies.

Additionally, it can be stated that the energetic potential for cold ambient conditions is reduced for the short driving cycles Load Case 5 and Load Case 6. In this case, the improved thermal management cannot make a significant benefit under usage of different

operating strategies due to the very short time (≈30 min). This behavior results from the thermal inertia of the system.

An evaluation of the optimized variables shows that the setpoint temperatures in warm ambient conditions are higher than in cold ambient conditions, which is explainable due to the functionality of the TMS. But, especially for cold ambient conditions, the setpoint temperatures differ between the individual Load Cases. One reason is the duration of the driving cycles; another is the driving dynamic of the cycle, especially when considering the self-heating of the drive system, which is higher under higher loads.

The conducted analyses demonstrate the potential for reducing total energy demand for two defined ambient temperatures, which represent the extreme values for the city of Hamburg. Further studies are examining intermediate temperatures with the goal of providing a comprehensive assessment of energy-saving potential. Therefore, three intermediate temperatures were evaluated, and the operating strategy of the thermal management system was optimized. Figure 13 shows the evaluation of the energy improvement $\Delta E_{el\,,\,Bat}$ as a function of ambient temperature, as well as the standard deviation as a function of the various driving cycles. It can be observed that the energetic improvement can be assumed to be linear and increasing as ambient temperatures rise. Furthermore, analysis of the standard deviation reveals a stronger influence of the Load cycle at higher ambient temperatures.

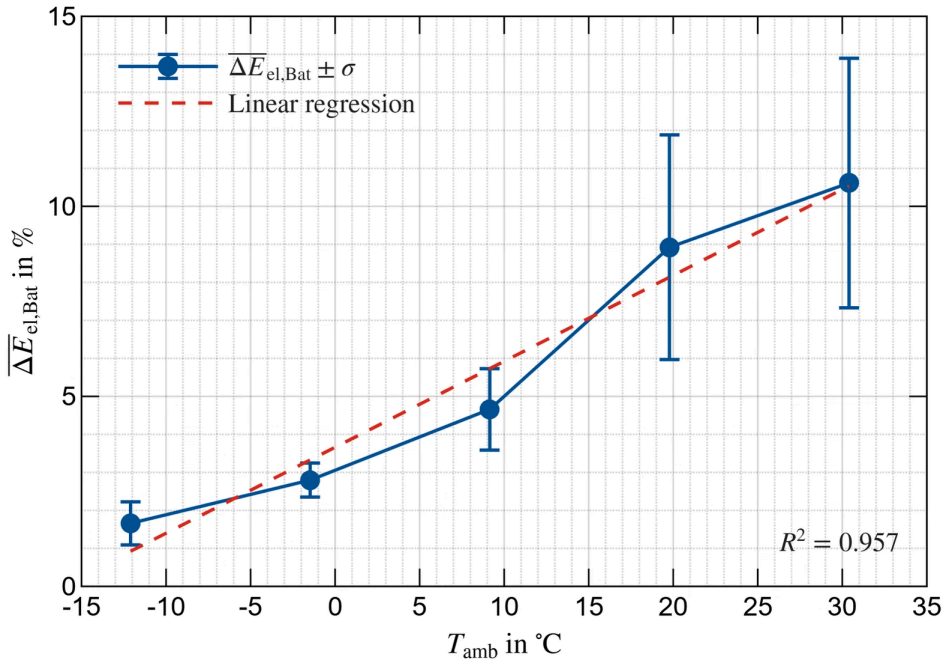


Figure 13. Energetic improvement by an optimized operating strategy of the thermal management system for intermediate ambient temperatures.

Finally, it should be noted that the calculated energetic potentials apply for individual drives that are started under the defined ambient conditions and without thermal preconditioning. Further investigations should be carried out regarding combinations of Load Cycles to consider preheated systems. To provide an overview of the capabilities of the proposed method, further analyses demonstrate the influence of combined driving cycles. To gain insight into energy savings on longer and more realistic bus routes, the six Load Cases were combined, and an optimization for extreme temperatures was performed. The results are presented in Table 7.

Table 7. Optimization results: potential energy savings by an optimized operating strategy in comparison to the baseline scenario for combined driving cycles.

Test Case	Optimized	Baseline	
	$E_{el,Bat}$ in kWh	$E_{el,Bat}$ in kWh	$\Delta E_{el,Bat}$ in %
Combination _cold	105.1329	105.8819	0.71
Combination_warm	71.5220	74.8174	4.40

6. Conclusions

The thermal management of BEVs shows potential to reduce their overall energy demand. Besides a reduction in greenhouse gas emissions, reduced energy demand causes an increased vehicle range. Especially in the field of electric city buses, the energy demand has an important role to fulfill the driving assignment. Due to its high predictability, daily circulations are tightly connected to the vehicle range. The present work proposes an optimized operating strategy for the thermal management of an electric city bus with the goal of reducing the overall energy demand. A method including the modeling of the thermal system in MATLAB/Simulink and Simscape calculates the thermal behavior of the system in high accuracy. Representative driving cycles and ambient conditions are extracted to reflect city bus operations in the city of Hamburg. An optimization using the Bayesian optimization algorithm yields an optimized operating strategy for the thermal management of the overall system depending on the specific driving profile and the ambient temperature. The optimization variables are the setpoints of the coolant inlet temperatures of the components ($T_{C,VEDS,in,SP}$, $T_{C,Bat,in,SP}$) as well as pump factors that correlate with the coolant flow rates in the components ($f_{pump,C,VEDS,in}$, $f_{pump,C,Bat,in}$). These parameters are set in the electronic control unit and can be adjusted depending on the concrete driving assignment. Therefore, a driving profile- and ambient temperature-based operating strategy can be defined. Summed up, a mean reduction of roughly 1.8% in cold ambient conditions and roughly 8.9% in warm ambient conditions in overall energy demand can be achieved for the described application. The method described can be used to optimize the system for additional driving cycles or ambient conditions. It is recommended to repeat the optimization under the adjusted conditions to obtain results for an energy-optimized operating strategy for the thermal management system.

Author Contributions: Conceptualization, H.S., T.H. and M.M.; methodology, H.S., T.H. and M.M.; software, H.S.; validation, H.S.; formal analysis, H.S.; investigation, H.S.; resources, M.M.; writing—original draft preparation, H.S.; writing—review and editing, H.S., T.H. and M.M.; visualization, H.S.; supervision, T.H. and M.M. All authors have read and agreed to the published version of the manuscript.

Funding: This research received no external funding.

Data Availability Statement: The data presented in this study are available on request from the corresponding author. Restrictions apply to the availability of these data. Data were obtained from external partners and are available from the authors with the permission of the partners.

Acknowledgments: The authors would like to thank Driventic GmbH and Eberspächer Sütrak GmbH & Co. KG for their support, particularly for providing access to their technical equipment and for their technical assistance in setting up the experimental setup.

Conflicts of Interest: The authors declare no conflicts of interest.

Abbreviations

The following abbreviations are used in this manuscript:

AF	Acquisition Function
BEV	Battery Electric Vehicle
BMS	Battery Management System
CAN	Controller Area Network
CoP	Coefficient of Performance
CV	Commercial Vehicle
DWD	Deutscher Wetterdienst
EI	Expected Improvement
fmi	Functional Mock-up Interface
GHG	Greenhouse Gas
GP	Gaussian Process
HVAC	Heating, Ventilation and Air Conditioning
LIB	Lithium Ion Battery
PAISI	Power and Inertia Simulator
SoC	State of Charge
SoH	State of Health
SP	Setpoint
TMS	Thermal Management System
VEDS	Voith Electrical Drive System
VIB	Vehicle Interface Box

Appendix A

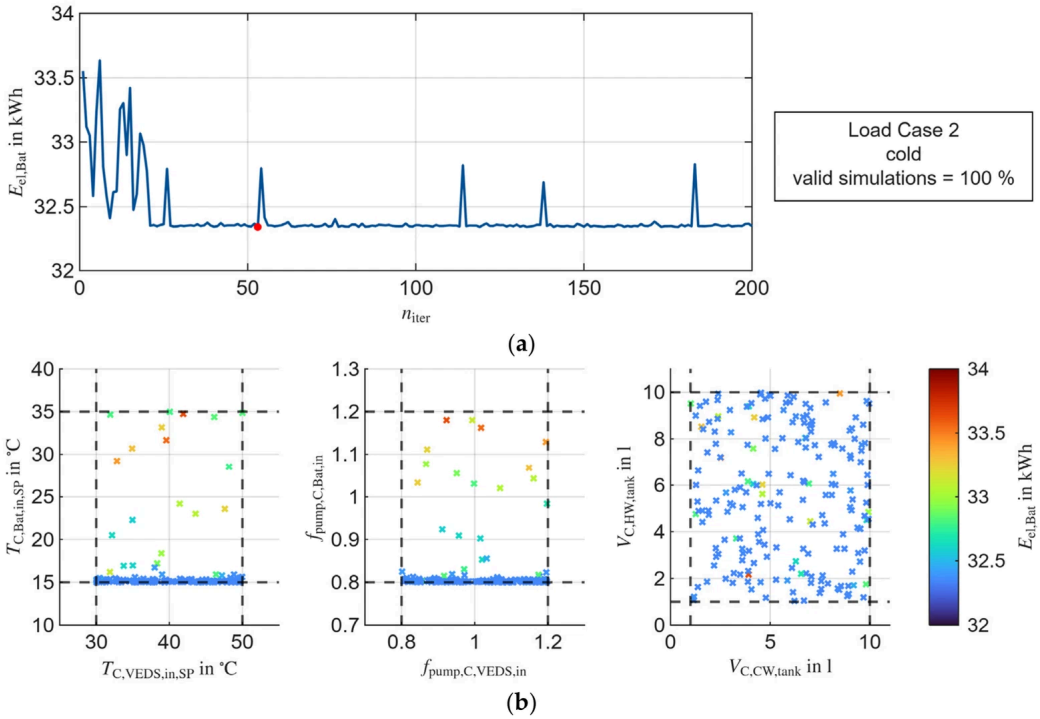


Figure A1. Results of the optimization for Load Case 2 at cold ambient conditions: (**a**) calculated

energy demand $E_{el,Bat}$ for all iterations; (**b**) energy demand $E_{el,Bat}$ depending on the different variable spaces.

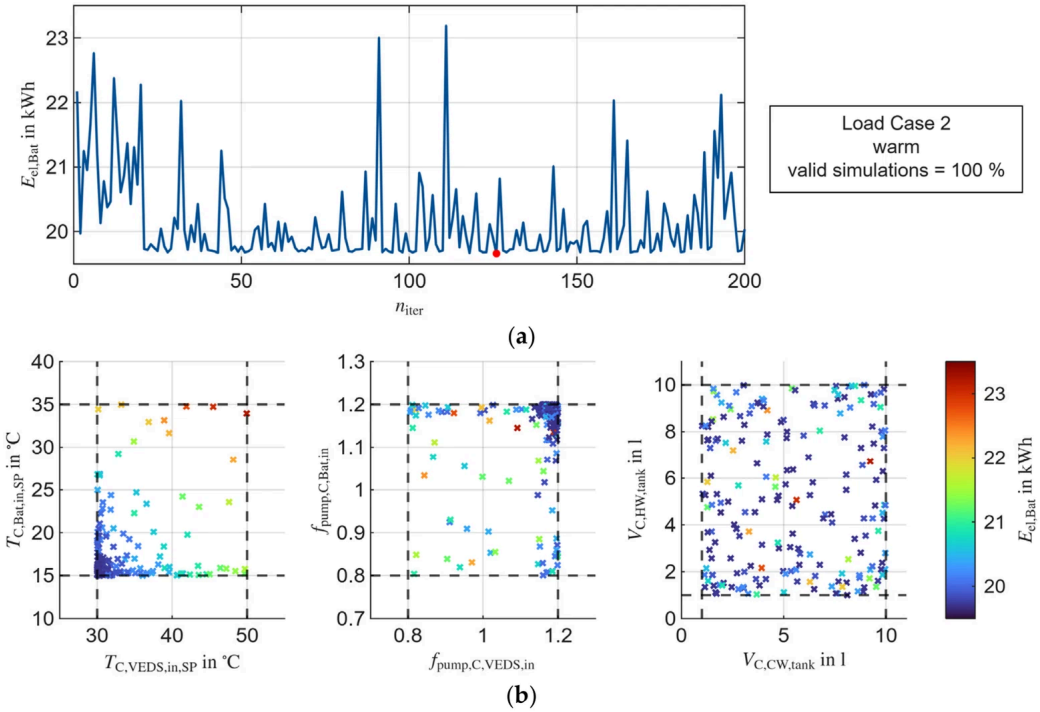


Figure A2. Results of the optimization for Load Case 2 at warm ambient conditions: (**a**) calculated energy demand $E_{el,Bat}$ for all iterations; (**b**) energy demand $E_{el,Bat}$ depending on the different variable spaces.

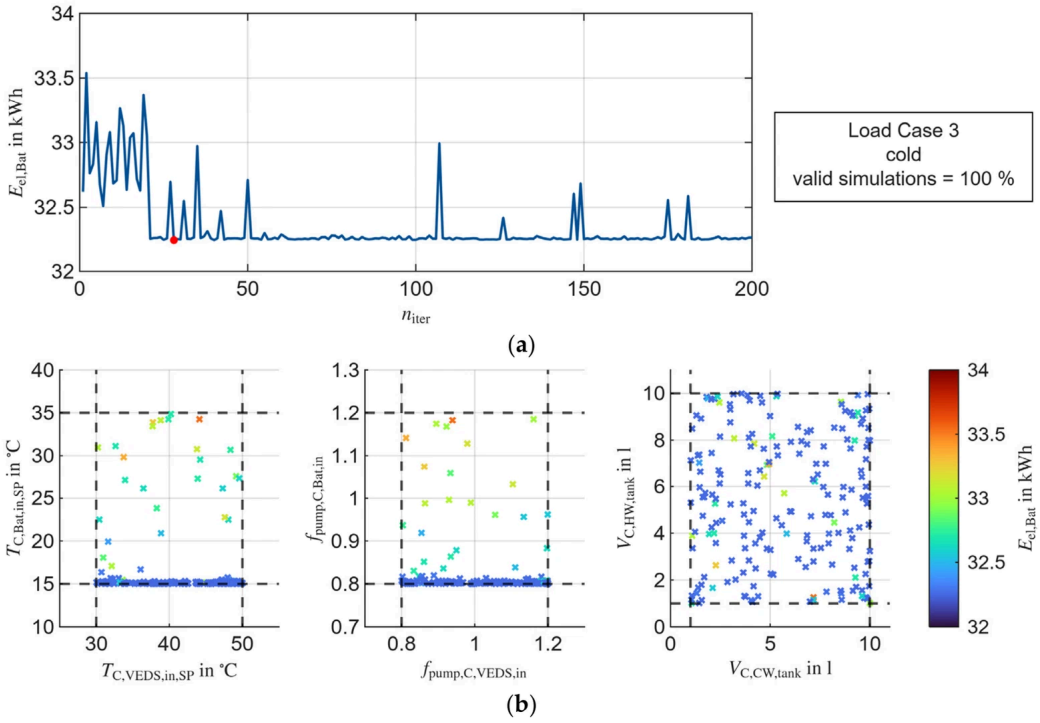


Figure A3. Results of the optimization for Load Case 3 at cold ambient conditions: (**a**) calculated

energy demand $E_{el,Bat}$ for all iterations; (**b**) energy demand $E_{el,Bat}$ depending on the different variable spaces.

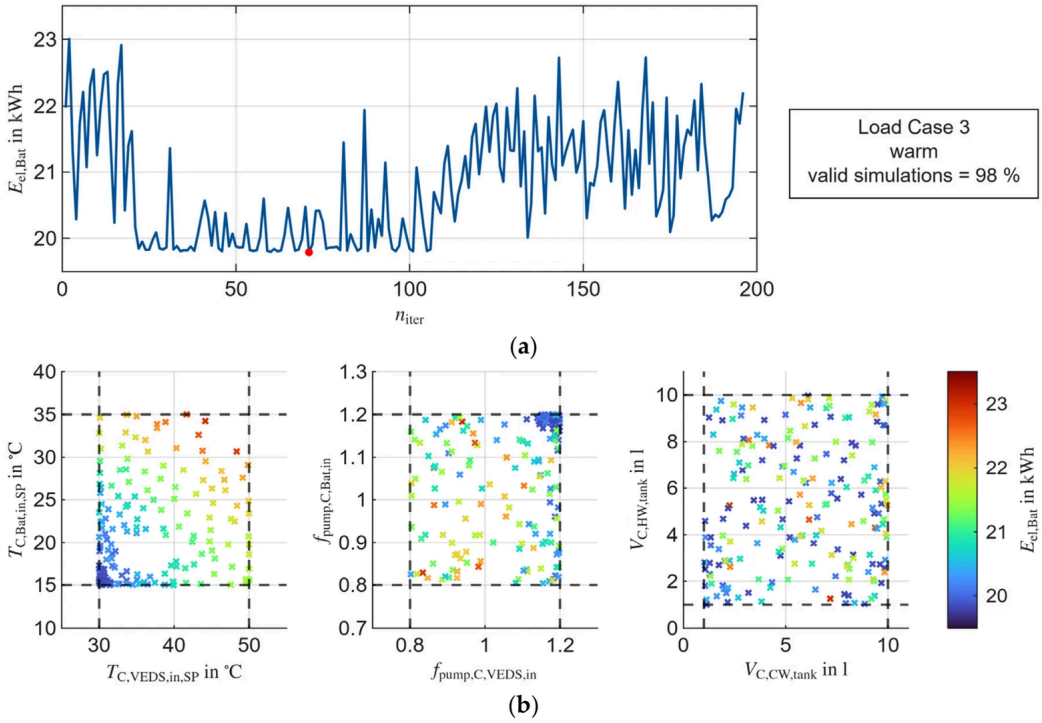


Figure A4. Results of the optimization for Load Case 3 at warm ambient conditions: (**a**) calculated energy demand $E_{el,Bat}$ for all iterations; (**b**) energy demand $E_{el,Bat}$ depending on the different variable spaces.

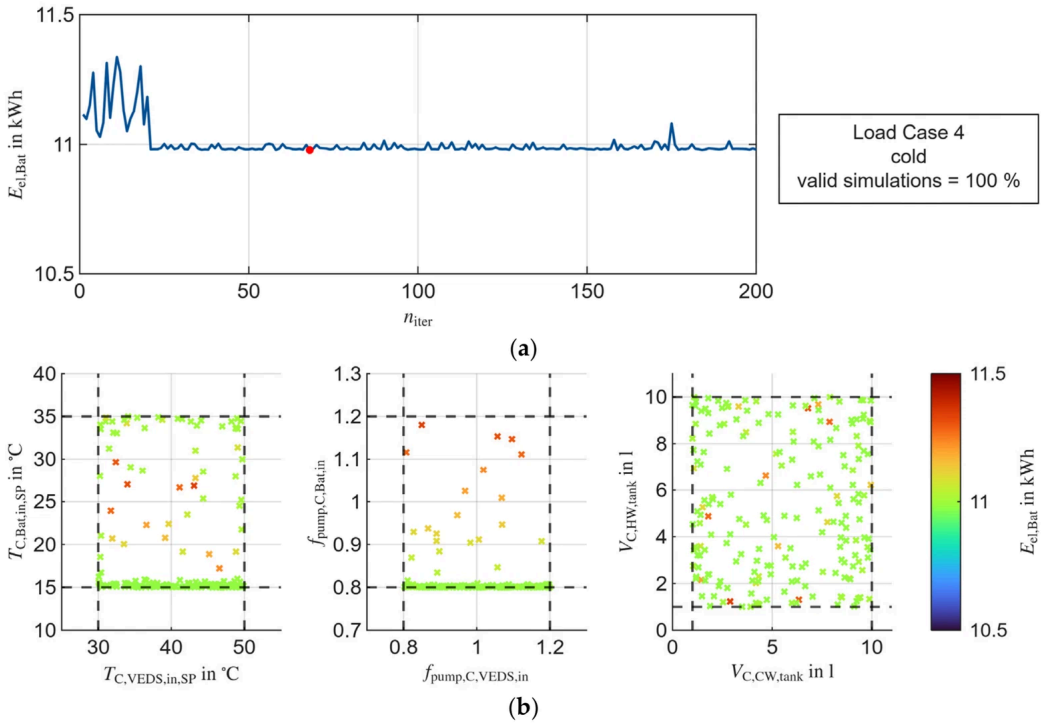


Figure A5. Results of the optimization for Load Case 4 at cold ambient conditions: (**a**) calculated

energy demand $E_{el,Bat}$ for all iterations; (**b**) energy demand $E_{el,Bat}$ depending on the different variable spaces.

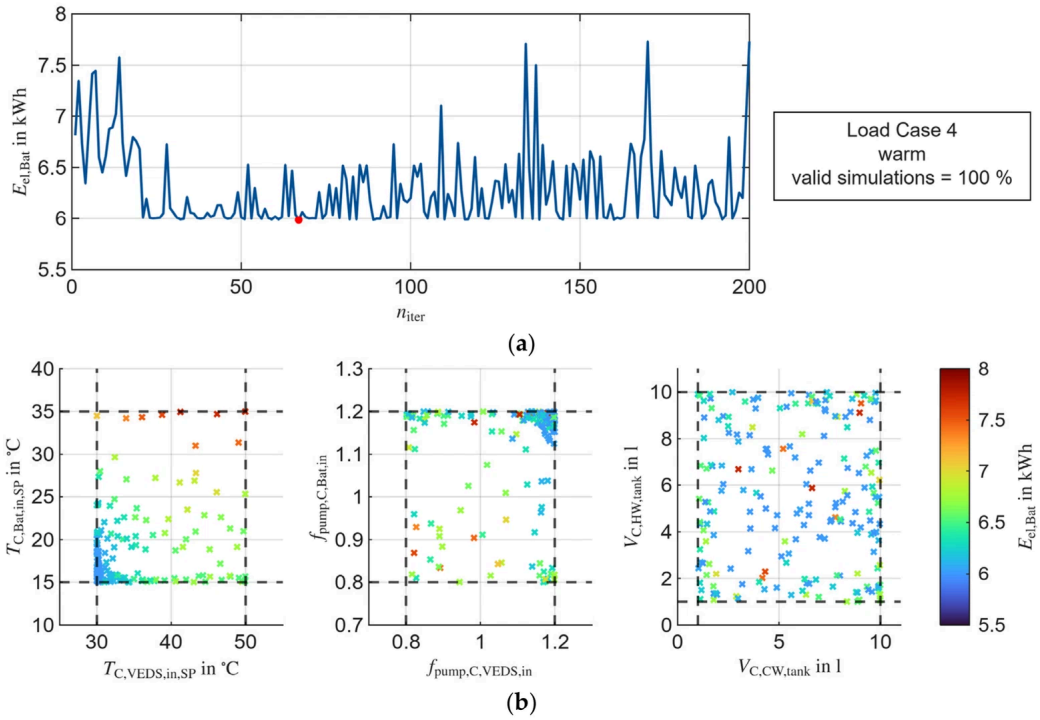


Figure A6. Results of the optimization for Load Case 4 at warm ambient conditions: (**a**) calculated energy demand $E_{el,Bat}$ for all iterations; (**b**) energy demand $E_{el,Bat}$ depending on the different variable spaces.

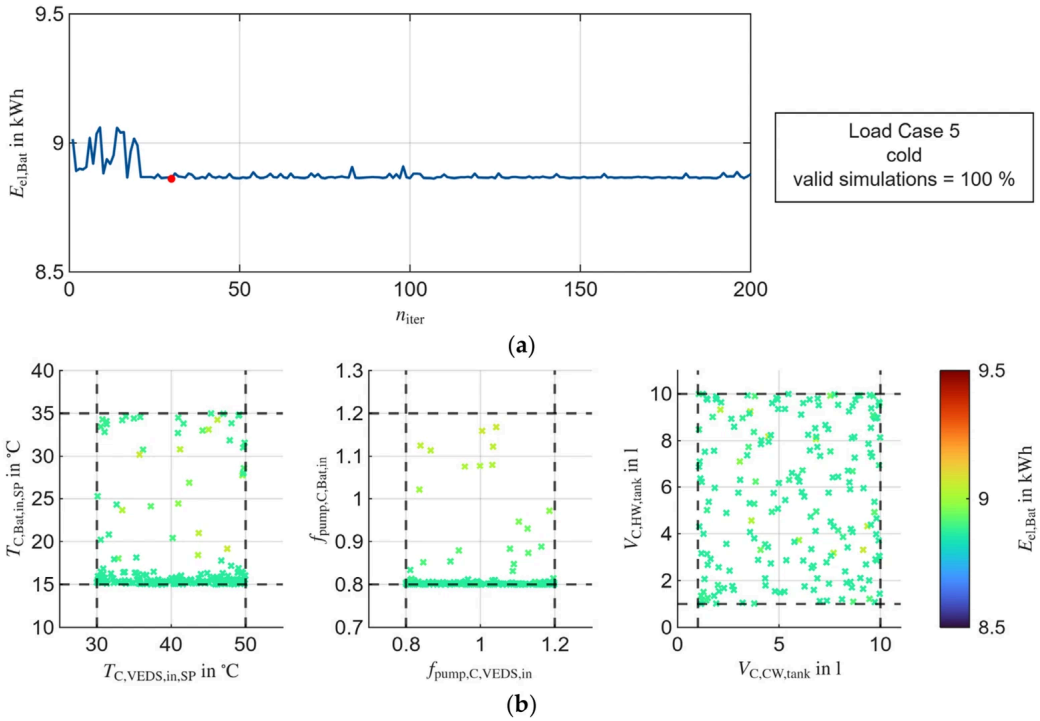


Figure A7. Results of the optimization for Load Case 5 at cold ambient conditions: (**a**) calculated

energy demand $E_{el,Bat}$ for all iterations; (**b**) energy demand $E_{el,Bat}$ depending on the different variable spaces.

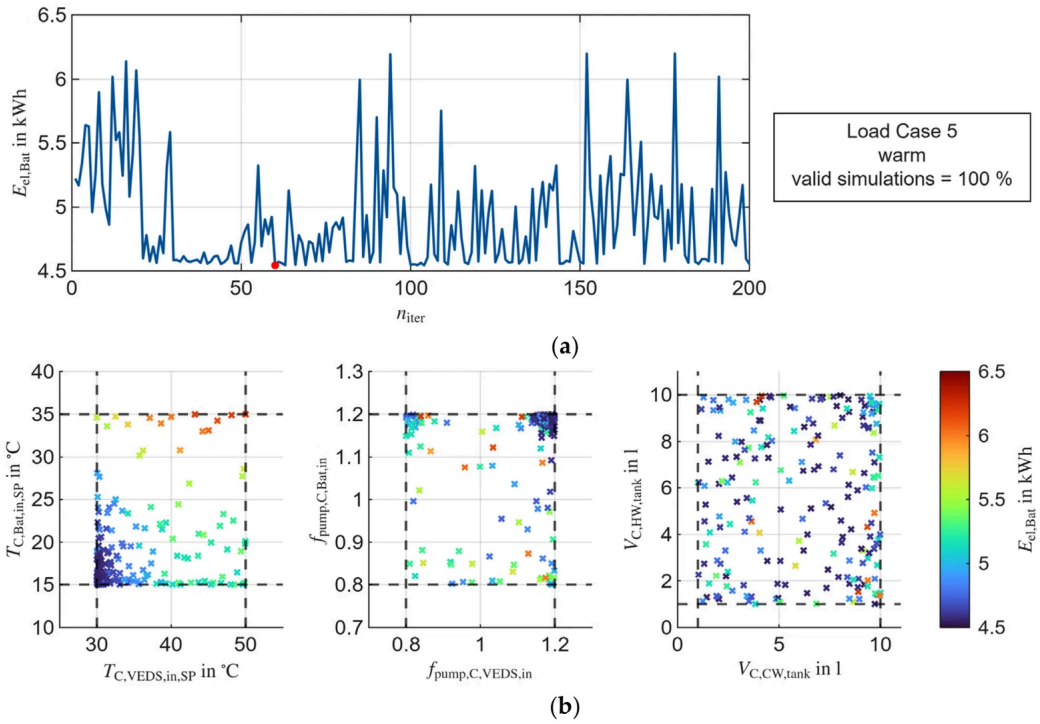


Figure A8. Results of the optimization for Load Case 5 at warm ambient conditions: (**a**) calculated energy demand $E_{el,Bat}$ for all iterations; (**b**) energy demand $E_{el,Bat}$ depending on the different variable spaces.

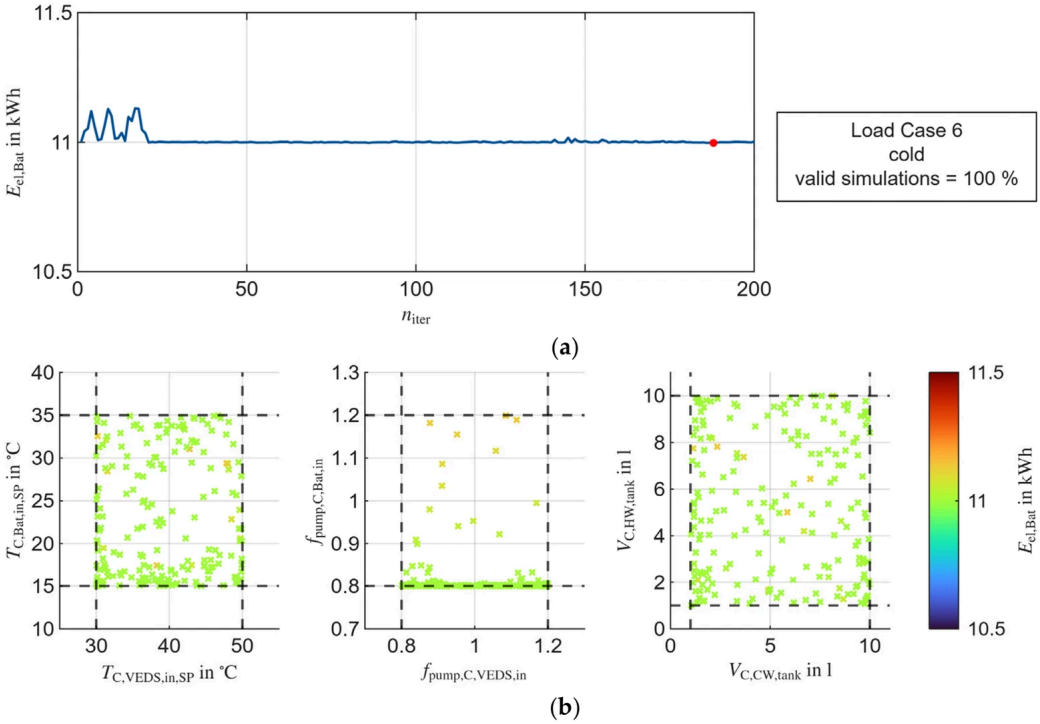


Figure A9. Results of the optimization for Load Case 6 at cold ambient conditions: (**a**) calculated

energy demand $E_{el,Bat}$ for all iterations; (**b**) energy demand $E_{el,Bat}$ depending on the different variable spaces.

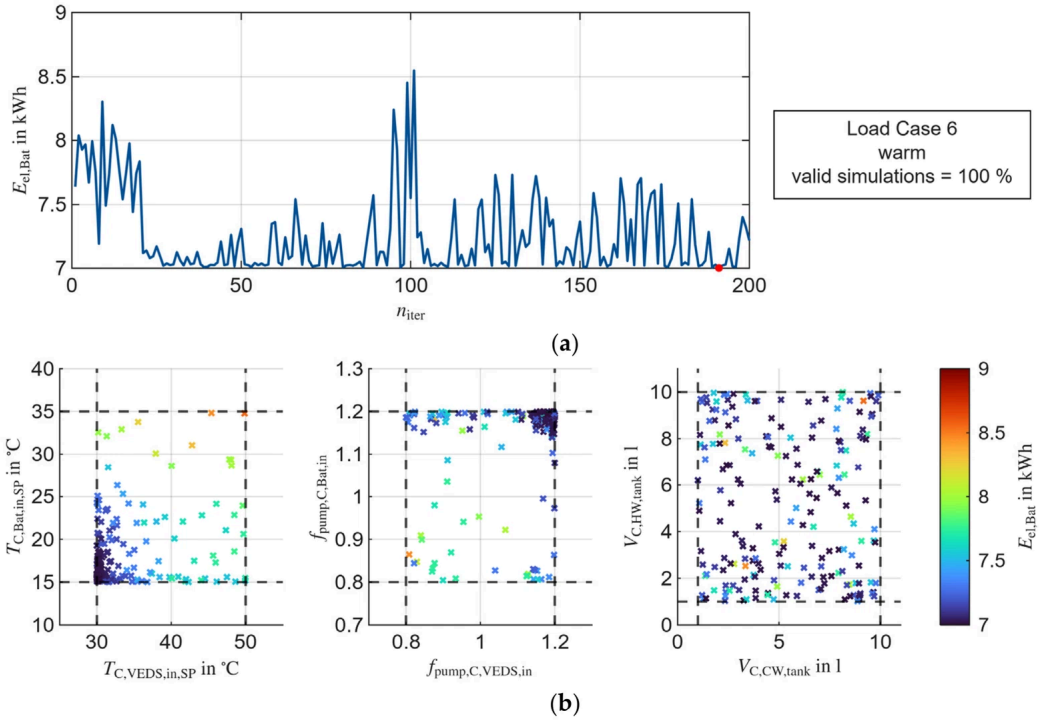


Figure A10. Results of the optimization for Load Case 6 at warm ambient conditions: (**a**) calculated energy demand $E_{el,Bat}$ for all iterations; (**b**) energy demand $E_{el,Bat}$ depending on the different variable spaces.

References

1. Ghosh, A. Possibilities and Challenges for the Inclusion of the Electric Vehicle (EV) to Reduce the Carbon Footprint in the Transport Sector: A Review. *Energies* **2020**, *13*, 2602. [Google Scholar] [CrossRef]
2. Wang, D.; Guo, J.; Zhang, Y.; Feng, T.; Chen, Z.-S.; Antwi-Afari, M.F.; Skibniewski, M.J. Optimizing electric vehicle charging-swapping schemes to enhance utilization of solar energy generation on highways. *Renew. Energy* **2026**, *270*, 125889. [Google Scholar] [CrossRef]
3. ACEA New Commercial Vehicle Registrations. Available online: https://www.acea.auto/cv-registrations/new-commercial-vehicle-registrations-vans-1-9-trucks-9-8-buses-22-7-in-h1-2026/ (accessed on 23 September 2026).
4. Al-Weikrat, Y.; Serrano, C.; Sodré, J.R. Effects of ambient temperature and trip characteristics on the energy consumption of an electric vehicle. *Energy* **2022**, *238*, 122028. [Google Scholar] [CrossRef]
5. Jahic, A.; Eskander, M.; Avdevicius, E.; Schulz, D. Energy Consumption of Battery- Electric Buses: Review of Influential Parameters and Modelling Approaches. *B&H Electr. Eng.* **2023**, *17*, 7–17. [Google Scholar] [CrossRef]
6. Li, B.; Kuo, H.; Wang, X.; Chen, Y.; Wang, Y.; Gerada, D.; Worall, S.; Stone, I.; Yan, Y. Thermal Management of Electrified Propulsion System for Low-Carbon Vehicles. *Automot. Innov.* **2020**, *3*, 299–316. [Google Scholar] [CrossRef]
7. Dabčević, Z.; Škugor, B.; Cvok, I.; Deur, J. A Trip-Based Data-Driven Model for Predicting Battery Energy Consumption of Electric City Buses. *Energies* **2024**, *17*, 911. [Google Scholar] [CrossRef]
8. Pesaran, A. Battery Thermal Management in EVs and HEVs: Issues and Solutions. In Proceedings of the Advanced Automotive Battery Conference, Las Vegas, NV, USA, 6–8 February 2001. [Google Scholar]
9. Ianniciello, L.; Biwolé, P.H.; Achard, P. Electric vehicles batteries thermal management systems employing phase change materials. *J. Power Sources* **2018**, *378*, 383–403. [Google Scholar] [CrossRef]

10. Steinstraeter, M.; Heinrich, T.; Lienkamp, M. Effect of Low Temperature on Electric Vehicle Range. *World Electr. Veh. J.* **2021**, *12*, 115. [Google Scholar] [CrossRef]
11. Auch, M.; Weyershäuser, K.; Kuthada, T.; Wagner, A. Reducing Temperature-Related Aging Inhomogeneities in Battery Modules Using a Switchable Thermal Management System. *SAE Int. J. Adv. Curr. Prac. Mobil.* **2025**, *7*, 2629–2649. [Google Scholar] [CrossRef]
12. Bandhauer, T.M.; Garimella, S.; Fuller, T.F. A Critical Review of Thermal Issues in Lithium-Ion Batteries. *J. Electrochem. Soc.* **2011**, *158*, R1–R25. [Google Scholar] [CrossRef]
13. Hoelle, S.; Scharner, S.; Asanin, S.; Hinrichsen, O. Analysis on Thermal Runaway Behavior of Prismatic Lithium-Ion Batteries with Autoclave Calorimetry. *J. Electrochem. Soc.* **2021**, *168*, 120515. [Google Scholar] [CrossRef]
14. Lupu, E.-D.; Tabacu, Ș.L.; Bobric, E.-C.; Irimia, D.; Vlad, V. Impact of thermal management and ambient temperature on aging of LFP, NMC, and NCA batteries for EVs. *EPJ Web Conf.* **2026**, *372*, 07009. [Google Scholar] [CrossRef]
15. Wu, H.; Chen, J.; Vaishnav, P.; Craig, M.T. Technological improvements in EV batteries offset climate-induced durability challenges. *Nat. Clim. Change* **2026**, *16*, 460–467. [Google Scholar] [CrossRef]
16. Zhu, Z.; Zhang, Y.; Chen, A.; Chen, J.; Wu, Y.; Wang, X.; Fei, T. Review of integrated thermal management system research for battery electrical vehicles. *J. Energy Storage* **2024**, *106*, 114662. [Google Scholar] [CrossRef]
17. Liu, G.; Ouyang, M.; Lu, L.; Li, J.; Han, X. Analysis of the heat generation of lithium-ion battery during charging and discharging considering different influencing factors. *J. Therm. Anal. Calorim.* **2014**, *116*, 1001–1010. [Google Scholar] [CrossRef]
18. Schröder, D. Verluste und Erwärmung im Antriebssystem. In *Elektrische Antriebe—Grundlagen*, 5th ed.; Springer Vieweg: Berlin/Heidelberg, Germany, 2013; pp. 44–79. [Google Scholar] [CrossRef]
19. Dan, D.; Zhao, Y.; Wei, M.; Wang, X. Review of Thermal Management Technology for Electric Vehicles. *Energies* **2023**, *16*, 4693. [Google Scholar] [CrossRef]
20. Kim, J.; Oh, J.; Lee, H. Review on battery thermal management system for electric vehicles. *Appl. Therm. Eng.* **2019**, *149*, 192–212. [Google Scholar] [CrossRef]
21. Wu, C.; Sun, Y.; Tang, H.; Zhang, S.; Yuan, W.; Zhu, L.; Tang, Y. A review on the liquid cooling thermal management system of lithium-ion batteries. *Appl. Energy* **2024**, *375*, 124173. [Google Scholar] [CrossRef]
22. Hou, P.; Ma, F.; Zhao, J.; Li, Y.; Wang, J.; Wei, H. A review on coupled system of topology optimization and phase change material for thermal management: Advances, challenges, and future perspectives. *J. Energy Storage* **2026**, *175*, 123262. [Google Scholar] [CrossRef]
23. Niu, W.; Pu, J.; Xu, Q. Research on integrated thermal management system for dual-motor electric vehicles based on heat pump air conditioning. *Heat Mass Transf.* **2026**, *62*, 88. [Google Scholar] [CrossRef]
24. Yang, G.; Xiao, G.; Pan, C.; Wu, J.; Jia, Z. Control Strategy of the Vehicle Thermal Management System for Battery Electric Vehicles Considering Energy Consumption Optimization. *Energies* **2026**, *19*, 2687. [Google Scholar] [CrossRef]
25. Rehm, D.; Krost, J.; Meywerk, M.; Czarnetzki, W. Optimized Cabin Heating Strategy for Battery Electric CEP Vehicles. In Proceedings of the 2025 Stuttgart International Symposium, Stuttgart, Germany, 2 July 2025. [Google Scholar] [CrossRef]
26. Guo, F.; Zhang, Z.; Mo, H.; Li, C. A Method for Battery SoH Estimation Based on K-means and LightGBM algorithm. In Proceedings of the 2024 6th International Conference on System Reliability and Safety Engineering: SRSE 2024, Hangzhou, China, 11–14 October 2024. [Google Scholar] [CrossRef]
27. Schäfer, H.; Hellberg, T.; Meywerk, M. Improved Thermal Management for Operating a Battery Electric City Bus under Real Driving Conditions. In Proceedings of the 2026 Stuttgart International Symposium, Stuttgart, Germany, 8 July 2026. [Google Scholar] [CrossRef]
28. Schäfer, H.; Meywerk, M.; Hellberg, T. Simulation-Based Investigation and its Experimental Validation of the Thermal Behaviour of a Battery Electric City Bus. *SAE Int. J. Adv. Curr. Prac. Mobil.* **2026**, *8*, 196–208. [Google Scholar] [CrossRef]
29. Meywerk, M. *Vehicle Dynamics*, 1st ed.; John Wiley & Sons: Chichester, UK, 2015; ISBN 978-1-118-97135-2. [Google Scholar]
30. Untersuchung des Rollwiderstands von Nutzfahrzeugreifen auf realer Fahrbahn. Available online: https://edocs.tib.eu/files/e01fn17/882141937.pdf (accessed on 23 September 2026).
31. Der eCitaro im Überblick. Available online: https://www.mercedes-benz-bus.com/de/de/models/ecitaro/facts-ecitaro.pdf (accessed on 23 September 2026).
32. Yuan, S.; Hofmann, W. Systematische Identifizierung energieeffizienter Antriebskonfigurationen in Elektrofahrzeugen. *Elektrotech. Inftech.* **2022**, *139*, 271–281. [Google Scholar] [CrossRef]

33. Schäfer, H.; Hellberg, T.; Meywerk, M. Simulation-Based Investigation and its Experimental Validation of the Thermal Behaviour of a BEV Bus. In Proceedings of the FKFS Conference on Vehicle Aerodynamics and Thermal Management, Leinfelden-Echterdingen, Germany, 15 October 2025. [Google Scholar]
34. Deutscher Wetterdienst Hamburg (Flugh.). Available online: https://www.dwd.de/DE/wetter/wetterundklima_vorort/schleswig-holstein_hamburg/hamburg/_node.html (accessed on 23 September 2026).
35. Benker, H. *Mathematische Optimierung mit Computeralgebrasystemen: Einführung für Ingenieure, Naturwissenschaftler und Wirtschaftswissenschaftler unter Anwendung von MATHEMATICA, MAPLE, MATHCAD, MATLAB und EXCEL*, 1st ed.; Springer: Berlin/Heidelberg, Germany, 2003. [Google Scholar] [CrossRef]
36. Roussel, R.; Edelen, A.L.; Boltz, T.; Kennedy, D.; Zhang, Z.; Ji, F.; Huang, X.; Ratner, D.; Santamaria Garcia, A.; Xu, C.; et al. Bayesian optimization algorithms for accelerator physics. *Phys. Rev. Accel. Beams* **2024**, *27*, 084801. [Google Scholar] [CrossRef]
37. Pelikan, M. Bayesian Optimization Algorithm. In *Hierarchical Bayesian Optimization Algorithm. Studies in Fuzziness and Soft Computing*; Springer: Berlin/Heidelberg, Germany, 2005; Volume 170. [Google Scholar] [CrossRef]
38. Shahriari, B.; Swersky, K.; Wang, Z.; Adams, R.P.; de Freitas, N. Taking the Human Out of the Loop: A Review of Bayesian Optimization. *Proc. IEEE* **2016**, *104*, 148–175. [Google Scholar] [CrossRef]
39. Chen, Y.; Chen, H.; Zeng, H.; Zhu, J.; Chen, K.; Cui, Z.; Wang, J. Structural optimization design of sinusoidal wavy plate fin heat sink with crosscut by Bayesian optimization. *Appl. Therm. Eng.* **2022**, *213*, 118755. [Google Scholar] [CrossRef]
40. Wang, X.; Jin, Y.; Schmitt, S.; Olhofer, M. Recent Advances in Bayesian Optimization. *ACM Comput. Surv.* **2023**, *55*, 1–36. [Google Scholar] [CrossRef]
41. Tatar, Ö.; Akgül, M.B.; Yurddaş, A. Cooling Performance Enhancement and Gaussian Process Regression-Based Multi-Objective Optimisation of a Weapon Turret Control Computer. *Energies* **2026**, *19*, 3409. [Google Scholar] [CrossRef]
42. Sarout, Y.; Jebahi, M.; Khelladi, S.; Nguyen, D.-V.; Scorsim, O. A Bayesian optimization-driven framework for CFD problems: Application to continuous casting. *Comput. Fluids* **2026**, *317*, 107185. [Google Scholar] [CrossRef]
43. Spearman, C. The Proof and Measurement of Association between Two Things. *Am. J. Psychol.* **1904**, *15*, 72–101. [Google Scholar] [CrossRef] [PubMed]

Disclaimer/Publisher's Note: The statements, opinions and data contained in all publications are solely those of the individual author(s) and contributor(s) and not of MDPI and/or the editor(s). MDPI and/or the editor(s) disclaim responsibility for any injury to people or property resulting from any ideas, methods, instructions or products referred to in the content.